frontiers | Frontiers in Earth Science

TYPE Original Research
PUBLISHED 30 October 2023
DOI 10.3389/feart.2023.1241975

OPEN ACCESS

EDITED BY
Paola Marianelli,
University of Pisa, Italy

REVIEWED BY
Miloš René,
Institute of Rock Structure and Mechanics (ASCR), Czechia
Alcides Pereira,
University of Coimbra, Portugal

*CORRESPONDENCE
Hesham M. H. Zakaly,
h.m.zakaly@gmail.com
Hamdy A. Awad,
hamdiawaad@gmail.com
Antoaneta Ene,
antoaneta.ene@ugal.ro

RECEIVED 18 June 2023
ACCEPTED 18 September 2023
PUBLISHED 30 October 2023

CITATION
Taalab SA, Zakaly HMH, Ivanov V, Alrowaily AW, Awad HA, Abed NS, Issa SAM, Eltohamy AM and Ene A (2023), Notable changes in geochemical and mineralogical characteristics of different phases of episyenitization: insights on the radioactive and shielding of the late phase.
Front. Earth Sci. 11:1241975.
doi: 10.3389/feart.2023.1241975

Notable changes in geochemical and mineralogical characteristics of different phases of episyenitization: insights on the radioactive and shielding of the late phase

Sherif A. Taalab[1], Hesham M. H. Zakaly[2,3,4]*, V. Ivanov[4], Albandari W. Alrowaily[5], Hamdy A. Awad[6]*, Neveen S. Abed[7], Shams A. M. Issa[2,8], Amira M. Eltohamy[7] and Antoaneta Ene[9]*

[1]Department of Geology, Faculty of Science, Al-Azhar University, Cairo, Egypt, [2]Department of Physics, Faculty of Science, Al-Azhar University, Assiut Branch, Assiut, Egypt, [3]Faculty of Engineering and Natural Sciences, Computer Engineering Department, Istinye University, Istanbul, Turkey, [4]Institute of Physics and Technology, Ural Federal University, Yekaterinburg, Saudi Arabia, [5]Department of Physics, College of Science, Princess Nourah Bint Abdulrahman University, Riyadh, Saudi Arabia, [6]Geology Department, Faculty of Science, Al-Azhar University, Assiut Branch, Assiut, Egypt, [7]Department of Geochemical Exploration, Nuclear Materials Authority, Cairo, Egypt, [8]Department of Physics, Faculty of Science, University of Tabuk, Tabuk, Saudi Arabia, [9]INPOLDE Research Center, Department of Chemistry, Physics and Environment, Faculty of Sciences and Environment, Dunarea de Jos University of Galati, Galati, Romania

Kab Amiri granites are submitted to post-magmatic hydrothermal solutions through fracture and faults, causing several alteration processes. The most common processes are episyenitization, saussuritization, hematitization, sericitization, kaolinization, albitization, chloritization, silicification, and muscovitization. Kab Amiri granites are vuggy, with the vugs partially to completely refilled with new constituents. The least episyenitized granites have elevated amounts of Fe, P, Zr, Ni, U, Th, Ba, Y, Hf, Nb, and As, which are correlated with their mobilization from biotite, k-feldspar, plagioclase and metamict zircon. These elemental changes are related the partial albitization, muscovitization, desilicification and chloritizatiom, which lead to the mobilization of these elements and forming of specific mineral association in the least altered granites such as autonite, tripiolite, columbite, Zircon and galena. On the second stage, granites were subjected to intense alteration processes by mineralizing fluids, causing wholly muscovitization of biotite and feldspar, albitization of plagioclase, carbonitization and apatitization. Many elements were mobilized from these altered minerals, including Ti, Al, Mn, Mg, Ca, Na, K, Mo, Cu, Pb, Zn, Ag, Co, Sr, V, Cr, Sn, Rb, Ta, Li, Sc, W, S, In, and Tl, leading to definite mineralization as kaslite, monazite, xenotime, polycrase and apatite. The mineralizing fluids in the least and highly episyenitized granites are incorporated in some ore minerals like uranophane, fergusonite, bazzite and garnet. Notably, the presence of elements such as U, Th, and other heavy metals in Kab Amiri granites highlights the potential for these rocks in radiation shielding applications.

The unique combination of elements and minerals resulting from the alteration processes can be leveraged for developing new materials or enhancing existing materials used in radiation shielding.

KEYWORDS

desilicified episyenite, bazzite mineral, isovalents, radiation shielding applications, dequartzification, rare earth elements, geochemistry, Kab Amiri

1 Introduction

The Kab Amiri area situated approximately 85 km from Qena. It is accessible via the Qena-Safaga asphalt road, leading into the desert through Wadi El-Missikat and eventually reaching Wadi Kab Amiri, which is about 40 km in length. The geographic coordinates of this region range between latitudes 26° 15′and 26° 25′N and longitudes 33° 30′and 33° 40′E (see Figure 1). Kab Amiri's granitic rocks form part of the Arabian-Nubian Shield constituting about 60% of exposed Neoproterozoic basement rock in Egypt's Eastern Desert and Sinai (El Bahariya, 2021). The area boasts two primary types of granitic rocks, distinguished by age and composition, with older rocks typically associated with subduction-related calc-alkaline affinities.

The region is renowned for its abundant granitic rocks, which play a crucial role in the construction industry worldwide. Often termed "granite," these rocks encompass various types, including those studied under igneous petrology and are widely used in construction due to their durability and aesthetic appeal (Hassan et al., 2019; Awad et al., 2020). Furthermore, granitic rocks in Kab Amiri have attracted the attention of researchers due to the presence of rare earth elements (REEs). These elements are indispensable for modern technologies such as metallurgy, defense systems, computer memory, mobile phones, wind turbines, energy-efficient lighting, and catalytic converters. The increasing demand for REEs is poised to strain existing supply chains (El-Taher et al., 2004).

Additionally, a noteworthy aspect of the granitic rocks in Kab Amiri is their potential application in radiation shielding. Given the dense and sturdy nature of granite, along with its compositional variety, there has been growing interest in investigating the viability of using these rocks for shielding against radiation. This is particularly relevant in contexts such as nuclear power plants, medical facilities, and space exploration, where radiation protection is critical. The granitic rocks from Kab Amiri, rich in heavy minerals (Taalab et al., 2023), could potentially offer better radiation attenuation properties (Tekin et al., 2018; Perişanoğlu et al., 2021; Saudi et al., 2021; Taalab et al., 2023). Evaluating the compositional variations and specific properties of these rocks may yield insights into the optimization of material selection for radiation shielding applications. Future studies should focus on the characterization of these granitic rocks regarding their density, composition, and effectiveness in attenuating various types of radiation.

Studies indicate that the granitoids of Kab Amiri show clear tetrad effects in chondrite-normalized REE patterns, a phenomenon often associated with secondary uranium mineralization on both local and global scales (Monecke et al., 2002; Mahdy and El-Kammar, 2003). These granites have also shown various types of

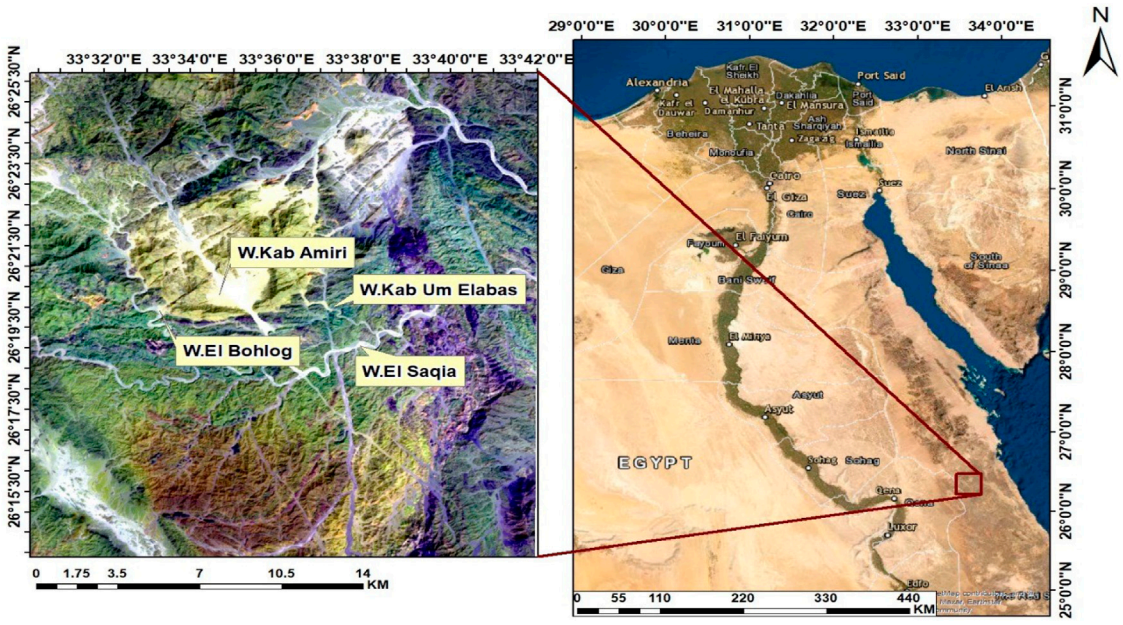

FIGURE 1
Landsat-8 ETM+ band 7, 6, 1 in R, G, B colors channels with location map in the Kab Amiri area of Egypt's Central Eastern Desert.

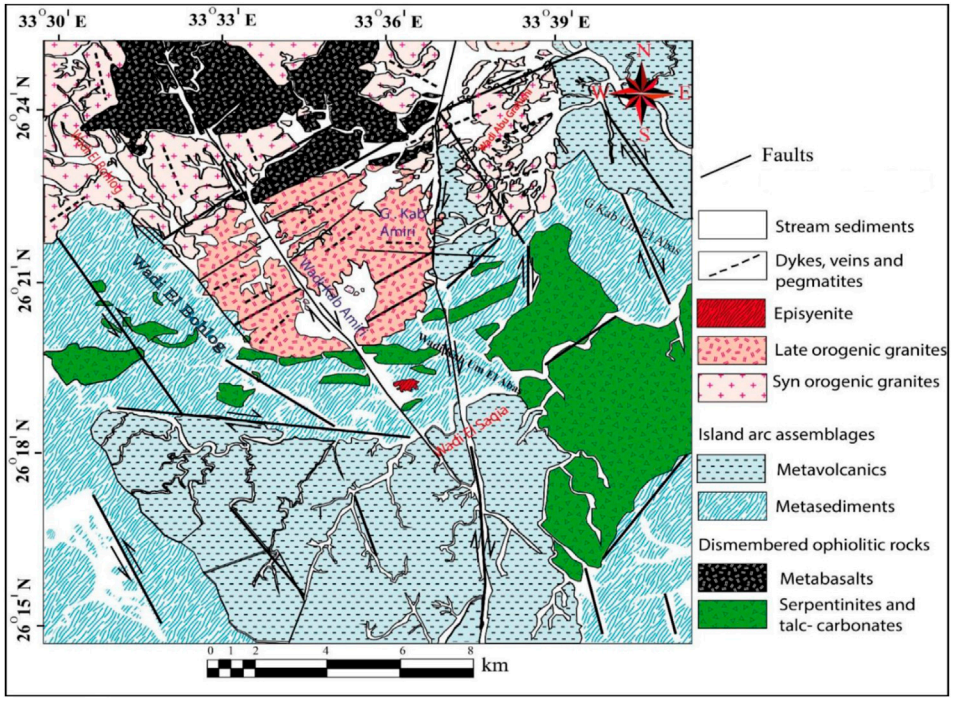

FIGURE 2
Geological map in the Kab Amiri area of Egypt's Central Eastern Desert (El Mezayen et al., 2022)

alteration, with episyenitization being one of the significant features. This alteration process creates porous rock (episyenite) through which later meteoric/hydrothermal minerals-rich fluids easily percolate, causing various types of episyenite. The purpose is to determine the precise relationship between the alteration processes and the resulting mineral associations. This is particularly important when considering radiation shielding applications, as the mineralogical composition of these granites may directly impact their radiation attenuation capabilities (Moghazy et al., 2021; Awad et al., 2022a; Abd El Rahman et al., 2022; El-Desoky et al., 2022). Additionally, exploring these granitic rocks may lead to discovering new, efficient materials for radiation shielding, thereby contributing to the broader field of radiation protection technology (Zakaly et al., 2021; Tekin et al., 2022). In the Kab Amiri area, four types of episyenitization have been identified: 1) spongy coarse-grain size granite, 2) spongy fine-grain size granite, 3) calcite episyenite and 4) speculative episyenite (Gaafar, 2005). These granitic rocks, which have undergone different types of alteration, possess unique mineral associations that are of interest from a geological perspective and have important implications in practical applications. These include chloritization, muscovitization, hematitization, sericitization, kaolinization, albitization, silicification, and saussuritization (El Mezayen et al., 2022). Each alteration introduces specific minerals and elements, which can alter the granite's properties, including its density and capacity for radiation attenuation (Zakaly et al., 2022; 2023). Moreover, the presence of mineral deposits, particularly those containing precious and base metals, is often associated with the hydrothermal alteration processes in these acidic rocks (El-Mezayen et al., 2015; Tarrah, 2016; Watanabe et al., 2018; Abdel-Rahman et al., 2022; Awad et al., 2022b; Taalab et al., 2023). The correlation between these minerals and hydrothermal alterations could provide key insights into the evolution of these granitic rocks and their properties, including radiation shielding potential.

The overarching aim of the study is to perform a comprehensive characterization of the least and most extensively desilicified episyenite, both geochemically and mineralogically. A deep understanding of the alteration processes and resulting mineral associations will yield insights into these granites' radiation shielding capabilities. Besides exploring the potential of these granites as radiation shielding material, this research could also lead to the development of innovative techniques for enhancing the properties of existing shielding materials. Such innovations could extend the life of shielding materials, reduce the cost, and increase the efficiency of radiation protection in various sectors such as nuclear power, healthcare, and space exploration. Therefore, the granitic rocks of Kab Amiri hold not just geological interest but also potential for significant practical applications.

2 Geologic setting

Kab Amiri area contains numerous rock units that can be grouped from oldest to youngest, as follows: serpentinites, talc-carbonates and metabasalts related to dismembered ophiolitic rocks; island arc assemblages represented by (metasediments and metavolcanics); these rocks were followed by granitoid rocks, which included episyenite, late orogenic and synorogenic granites, basaltic and aplitic post-granitic dykes, pegmatite, quartz veins, and stream sediments are all examples of granites (Figure 2).

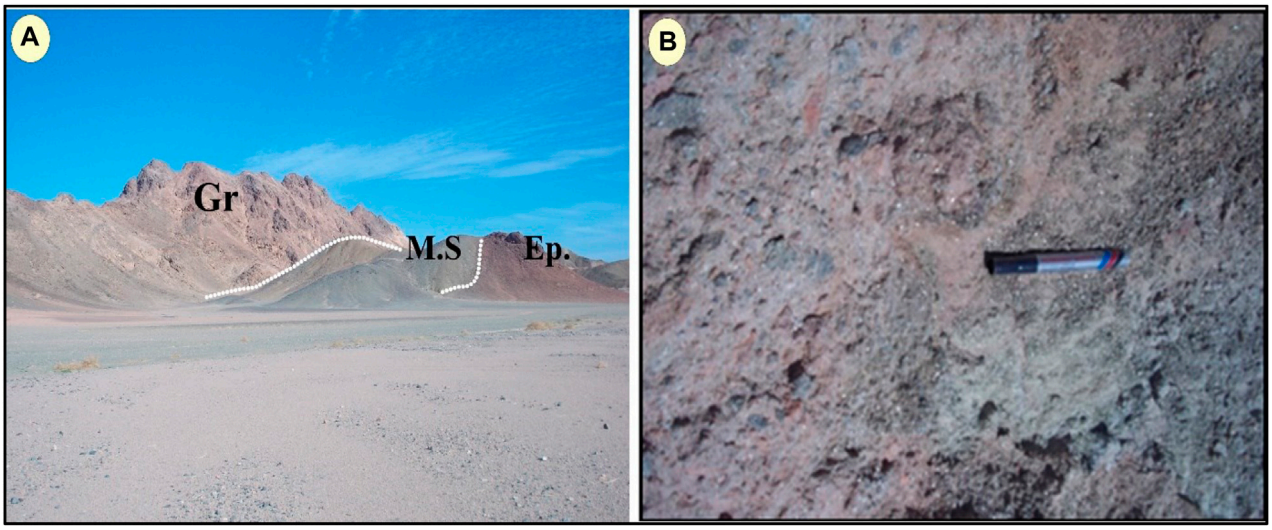

FIGURE 3
Macrophotographs of **(A)** Episyenite (Ep.) intruding the metasediments (M.S). **(B)** Radioactive mineralized spongy episyenite showing dequartizification vugs, muscovitization, and hematitization.

Aerial photos, Thematic Mapper Lands at pictures, extensive fieldwork, and more than a hundred samples gathered from the area were used to create a geologic map of the study area at a scale of 1:50,000 (Figure 2). During progress in our study for Kab Amiri area, we noticed that the late orogenic granites which are encountered in the central part of the map, as two separated blocks cut by Wadi Kab Amiri. We found out that these altered granites represent the first stage of episyenite and have two different stages of episyenitization; the first is the least altered, while the second one is the highly altered. This large variation was confirmed in the field studies, and we recorded the presence of the two types with gradational contact. These two types are variable petrographically, chemically, in mineral association and radiometrically. This discovery were recorded for the first type. The notable variability in their characterization lead us to make more investigations to detect their shielding properties, and our work have not any relation to what we previously published.

The second stage of Episyenite is part of the post-orogenic granite of the pluton Kab Amiri subjected to alkaline metasomatism. It emerges from the metasediments at a distance of 1.5 km from the southern edge of the Kab Amiri granite pluton. With the metasediments, it exhibits abrupt intrusive contact (Figure 3A). In the field, the epiyenite body has an oval shape form of approximately 0.7 km in diameter, showing moderate relief. It is highly faulted and fractured in NW, NE, and E-W trends. This rock is medium-grained, pink, and mostly mucovitized and hemititized. It shows a spongy shape due to dequartizification vugs and is mostly radioactively mineralized (Figure 3B). The hydrothermal alterations are structurally controlled, that different types of alterations are restricted along and around those main trends, namely, desilicification, albitization, greisenization, chloritization, carbonitization and hematitization. The hydrothermal leaching of quartz from granite is frequently associated with sodium and/or potassium metasomatism, promoting important alterations in the primary mineralogy and concomitant changes in the whole rock composition. The differential stability of granite minerals other than quartz during alteration and the variety of vug infillings explains the range of the observed chemical changes. (Gaafar, 2005) reexplains the range of the observed chemical changescognized three types of episyenitization in the Kab Amiri area:

1- Episyenite, with free vugs, represent the most common outcropping type with a highly weathered surface and forms the lowest elevation. This type of episyenite may act as a trap for uranium mineralization.
2- Episyenite, with vugs filled with calcite, is dominant at the western part of the main episyenitized zone. The highest radioactive spot. The occurrence of calcite filling in episyenite is a strong indication of the carbonate complex bearing solutions, which may have transported uranium in solution. Such carbonate-filled episyenite commonly occur at the periphery of uranium-mineralized episyenites.
3- Massive episyenite with very limited or no vugs and higher Th (Max. 40.3 ppm) and K (Max. 7 wt%) contents. Such episyenites have limited occurrence. They contain secondary Iron oxides, and/or orthoclase and/or albite due to potassium and/or sodium metasomatism and commonly occur at the east of the main episyenitized zone.

This episyenite represents a favourable reservoir for uranium mineralization due to its large empty volume (up to 30%). These vugs are not filled with early magnetic minerals such as albite and thus may have been filled by uranium mineralization, subsequently leached by hydrothermal and/or meteoric solutions in the upper tens or more meters of the episyenite body (Abdel Meguid et al., 2003).

3 Methodology

The methodology involved a comprehensive examination of eight thin sections of episyenite using a polarizing microscope to

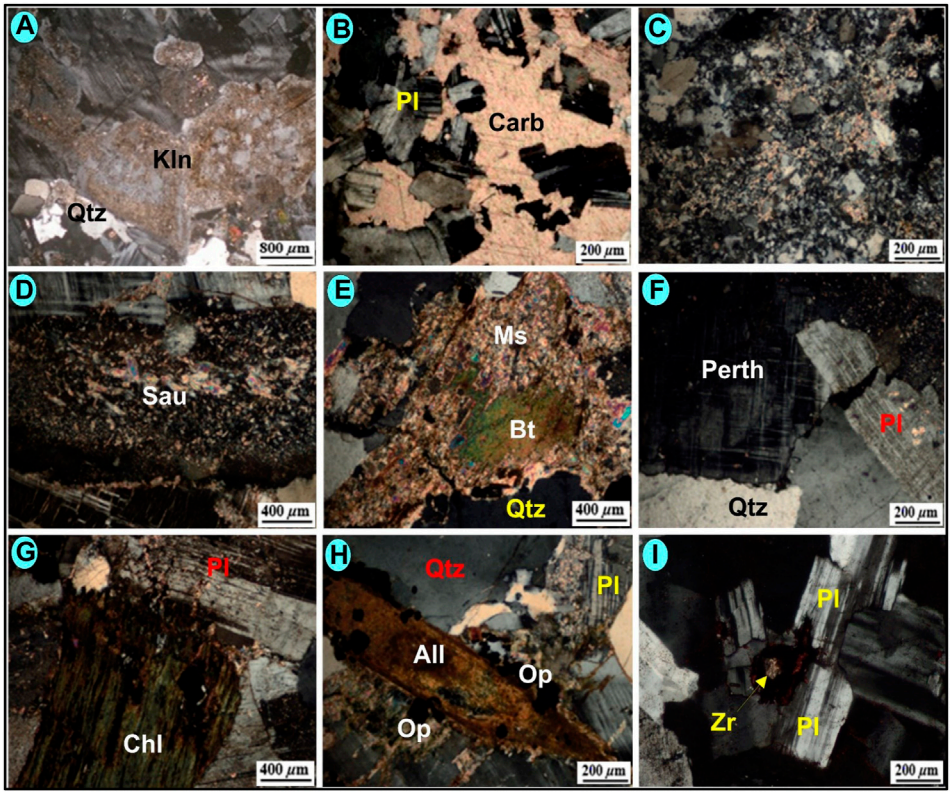

FIGURE 4
Photomicrographs for the least desilicified episyenite of Kab Amiri showing: **(A)** Kaolinitized perthite, CN. **(B)** Dissolution of plagioclase and refilling by secondary carbonate (Car), CN. **(C)** Reworked silica as thermal effect of hydrothermal solution, CN. **(D)** Saussiritization of plagioclase, CN. **(E)** Muscovitization (Ms) of potash metasomatism, CN. **(F)** perthite texture and microcline structure, CN. **(G)** chloritization of biotite, CN. **(H)** long crystal of allanite, CN. **(I)** Minute crystal of metamict Zircon coated by iron oxides in plagioclase, CN.

determine their mineralogical composition and texture. Following this, selected episyenite samples were subjected to a process to isolate their heavy mineral fraction. Initial processing involved crushing, grinding, quartering, and sieving the samples to a mesh size fraction of −60 to +120. Subsequently, a bromoform heavy liquid with a specific gravity of 2.85 gm/cm^3 was employed to concentrate the heavy minerals. Magnetite present in the samples was initially separated using a hand-magnet and further segregated from the heavy mineral fractions using a Frantz Isodynamic Magnetic Separator Model L-1. The device was operated with a side tilt of 5° and a forward slope of 20°, generating numerous magnetic fractions at 0.2, 0.5, 0.7, 1, and 1.5 A. Post-separation, minerals were identified using both an environmental scanning electron microscope (ESEM) and a binocular microscope. Furthermore, an energy dispersive spectrometer (EDX) unit complementing the ESEM model Philips XL 30 was used at 25–30 kV accelerating voltage, a 1–2 mm beam diameter, and 60–120 s counting duration. This process ensured precision, especially during the ESEM-EDX analyses, with a specific focus on areas close to the grain centers to minimize electron beam diffraction at the grain borders.

Inductively coupled plasma emission spectrometry (ICP-ES) was utilized following a lithium metaborate/tetraborate fusion and dilute nitric digestion for a comprehensive chemical examination of whole-rock samples. This process occurred at ACME Analytical Laboratories Ltd., Vancouver, Canada. The quantities of rare earth elements in the samples were determined using inductive coupled plasma mass spectrometry (ICP-MS) at the same facility. Major oxide detection limits ranged from 0.001 weight percent to 0.04 weight percent, and trace element detection limits varied between 0.01 and 0.5 ppm. The precision of this analysis, verified by repeat analyses, varied from 2% to 20% for trace elements and 0.5% for major elements. Furthermore, to ascertain the loss of ignition (L.O.I), 1 g of each sample was heated at 950°C for 90 min. In addition, the shielding parameters of these samples were determined utilizing the NISTXCOM photon cross sections database. This computational analysis served to understand the potential of the Kab Amiri granites for radiation shielding applications, providing a critical basis for the prospective use of these granites in various radiation-intensive industries.

4 Results

4.1 Petrographic inspection of episyenite

Two different types of episyenitized granites can be found in the research area; the first is the least desilicified granite, and the second is the most desilicified granite. The major pluton of post-orogenic

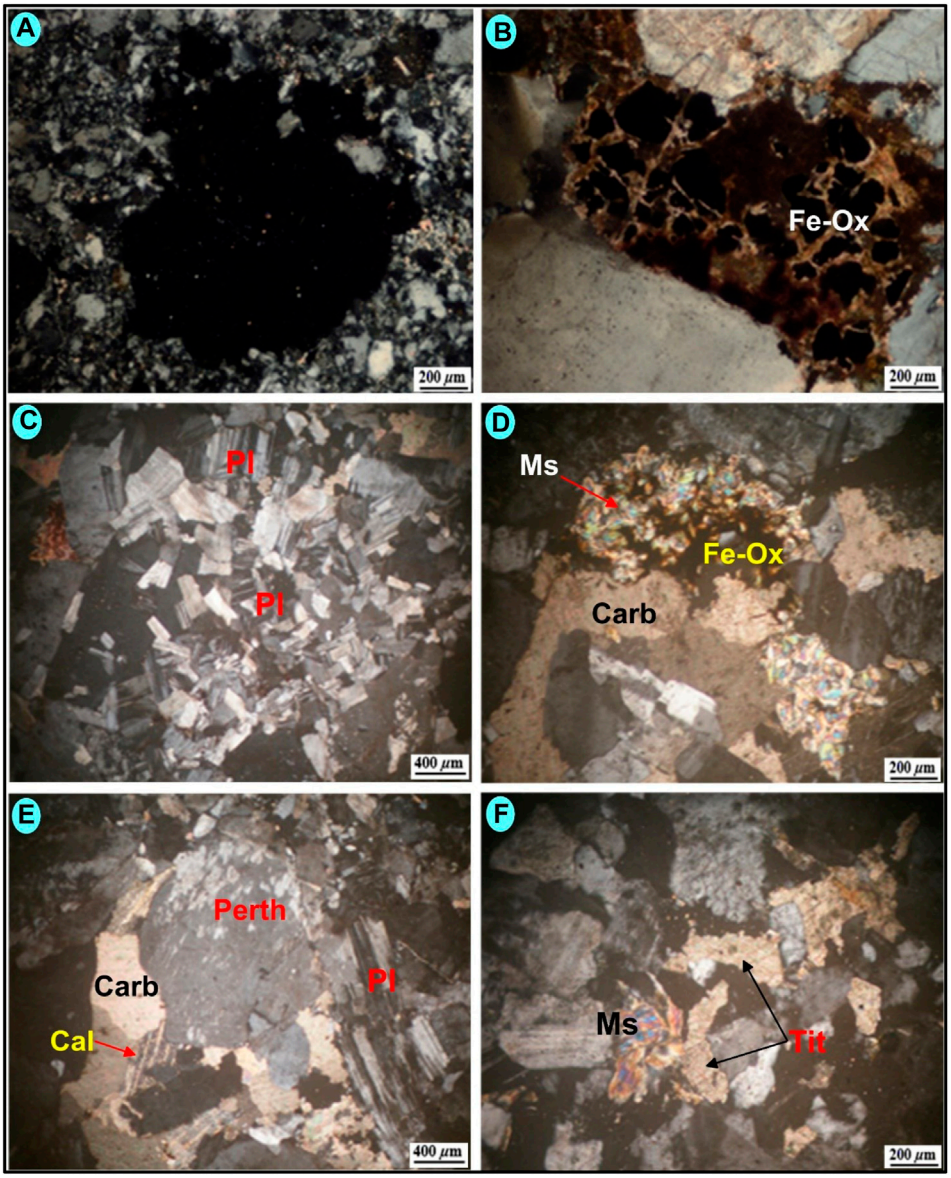

FIGURE 5
Photomicrographs showing the occurrence of secondary minerals in vugs of the highly desilicified episyenite of Kab Amiri: **(A)** Vug is created by the dissolution of silicate minerals, CN. **(B)** Vug filling by secondary iron oxides (Fe-Ox), CN. **(C)** Vug filling by secondary albite (Fe-Ox), CN. **(D)** radial shape of muscovite surrounded by carbonate and opaque mineral, CN. **(E)** Platy calcite partly includes carbonate and perthite microcline in a vug, CN. **(F)** Secondary titanite and muscovite filling Vugs, CN.

granites that have been sheared and hydrothermally changed is typified by the least desilicified episyenite, especially where it meets metasediments rock. The highly desilicified granites (episyenite) are the little stock-like episyenite bodies that invade metasediments. Parts per million (ppm) and weight (% by weight), respectively.

The least desilicified episyenite rock in Kab Amiri area is medium to coarse-grained with porphyritic, sometimes poikilitic texture characterized by pink-red K-feldspar, white plagioclase, muscovite, biotite and quartz as essential minerals. Zircon and allanite are the main accessory minerals; the secondary minerals are carbonates, muscovite, and Chlorite. Albite can take the place of plagioclase and k-feldspar. Outside of the episyenite bodies, moderate albitization of k-feldspars also occurs in the granite (Figure 4A). These rocks have remnants of unaltered K-feldspar, suggesting that they were not previously albitized. The plagioclase is also dissolved in the hydrothermal solution where the cavities are refilled by secondary carbonate (Figure 4B). The effect of the hydrothermal solution may cause mild processes of alteration expressed as a reworking of silica (Figure 4C) and saussuritization of plagioclase (Figure 4D). The absence of primary muscovite may illustrate its late-magmatic origin and could be disturbed later by post-magmatic alteration (Figure 4E). K-feldspar still preserves perthite texture and microcline structure (Figure 4F). Chlorite occurs as pseudomorphic after biotite and may be protected partly during later hydrothermal alteration in least desilicified episyenite (Figure 4G). The studied least desilicified

TABLE 1 The recorded minerals in the highly and slightly altered Kab Ameri episyenite.

Mineral		Rock type	
		Highly altered	Slightly altered
Radioactive minerals	Kasolite	√	
	Uranophane	√	√
	Autunite		√
	Uranothorite	√	√
Rare earth bearing minerals	Monazite	√	
	Xenotime	√	
Nb-Ta minerals	Tapiolite		√
	Columbite		√
	Polycrase	√	
	Fergusonite	√	√
Accessory minerals	Bazzite	√	√
	Zircon		√
	Fluorite		√
	Cotunite		√
	Galena	√	
	Apatite		√
	Garnet	√	√

episyenite encloses accessory minerals such as allanite which is considered a Ce-rich mineral. It is present as a long crystal with yellowish-brown colour characterized by high relief and masked interference colour. It encloses pleochroic halos as an indication of the presence of a radionuclides (Figure 4H). Zircon is another accessory mineral that is recorded as a minute crystal associating the plagioclase. The crystal is intensively metamectized, where it loses its interference colour, coated by the iron oxides, causing fracturing and hematitization for the surrounding plagioclase (Figure 4I). These microscopic features are indicative of the presence of the radioelements.

Highly desilicified episyenite rock shows white feldspars due to albitization or sericitization and when compared to the fresh (host) granite, episyenite is clearly porous and whitened. It is further distinguished by the absence of magmatic quartz. It is medium to coarse-grained rock characterized by a pink-red colour and the abundance of vugs (due to the dissolution of quartz), which are filled with carbonate. Microscopically, secondary minerals such as quartz, opaques, albite, muscovite, and calcite are identified as filling minerals in the vugs. Quartz is the most susceptible mineral to the process of episyenitization due to its low-temperature degrees of remelting or recrystallization. The constituting quartz is dissolved by the hydrothermal solutions causing cavities that are maintained as vugs (Figure 5A) or refilled by other materials such as iron oxides (Figure 5B). In vugs of albitized episyenite, some anhedral to euhedral authigenic albite was seen (Figure 5C). White mica formed after quartz leaching and before the crystallization of the carbonate that filled the vugs, forming tufts of muscovite that were radial in shape (Figure 5D). The core of the sample shows platy crystals throughout the vugs, demonstrating the prevalence of this calcite crystal in vugs (Figure 5E). These platy calcite crystals contain some carbonate and perthite microcline (Figure 5F). shows the secondary titanite and muscovite in the vugs of the episyenite.

4.2 Mineralogical studies of episyenite

The ESEM data and the mineralogical analysis of the slightly and highly altered episyenite showed that the following mineral groups were registered (Table 1).

4.2.1 Radioactive minerals

4.2.1.1 U-Silicates

4.2.1.1.1 Uranophane [Ca $(UO_2)_2(SiO_3OH)_2.5H_2O$]. The most common type of calcium uranium silicate is uranophane, which is produced when uraninite is weathered by oxidation-hydration in settings with high concentrations of Si^{4+} (Krivovichev et al., 2013; Plasil, 2014). The monoclinic system is where uranophane crystallises, and several colours, for instance, straw yellow, orange-yellow, yellow, and canary yellow. With different gradations and dull and greasy luster with a hardness on the Moho scale, 2–3. Uranophane grains occur as massive, soft, radiated aggregates, microfractures filling or coating on feldspars. Binocular microscope image, (SEM/EDX) analysis, and (BSE)

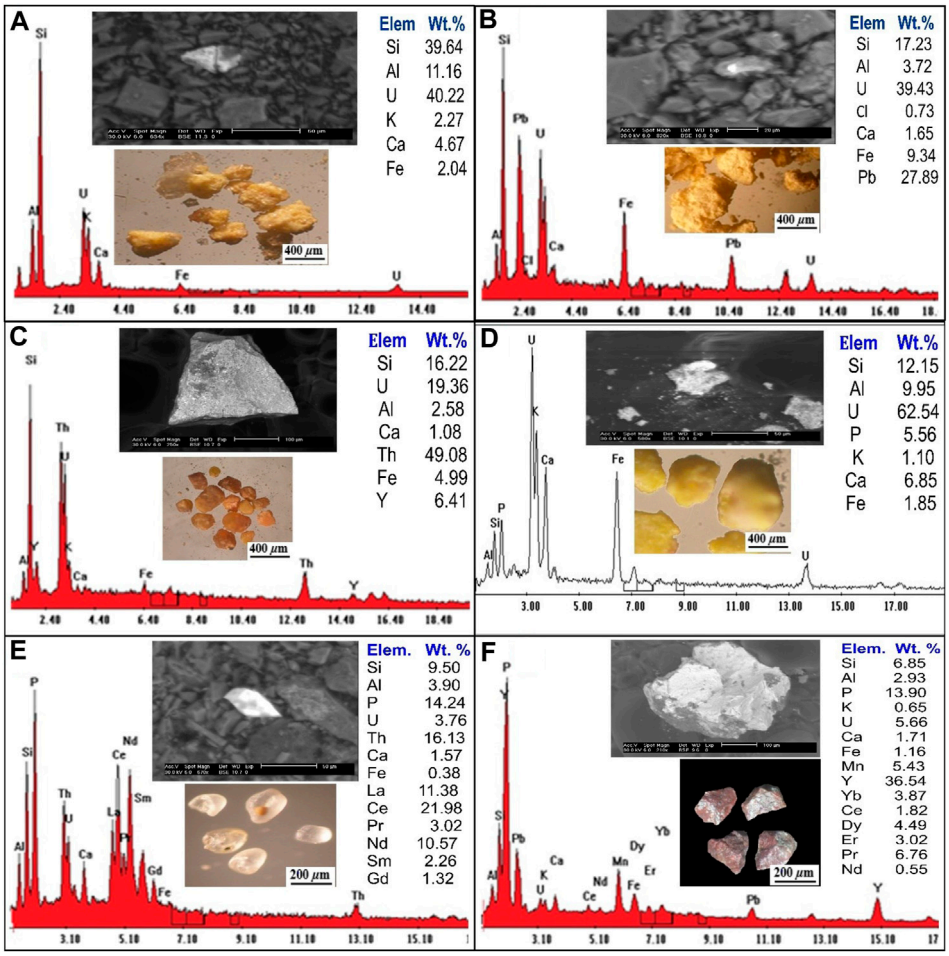

FIGURE 6
Binocular microscope images, EDS analysis and BSE images for **(A)** Uranophane mineral; **(B)** Kasolite mineral; **(C)** Uranothorite mineral; **(D)** Autunite mineral; **(E)** Monazite mineral; **(F)** Xenotime mineral.

(Figure 6A) reveal that uranophane grains consist mainly of U (40.22%), Si (39.64%), Ca (4.67%), Al (11.16%), K (2.27%) and Fe (2.04%).

4.2.1.1.2 Kasolite [Pb (UO_2) (SiO_4) (H_2O)]. (Schoep, 1921) made the first discovery of the significant hydrated uranyl silicate mineral phase known as kasolite. Kasolite is the only known uranyl silicate that contains lead, together with the lead uranyl oxides (Pb (UO_2) (SiO_4). H_2O). Kasolite is less abundant than uranophane. It is distinguished by a monoclinic system and bright colours (canary lemon, brown and yellow at different intensities), and greasy luster. Kasolite occurs as small prismatic aggregates recorded in the episyenite samples and sometimes occurs as stains along with fractures. SEM/EDX and (BSE) (Figure 6B), the kasolite EDX analytical results show the presence of U (39.43%), Si (17.24%) and Ca (1.65%), Al (3.72%), Pb (27.89%), Fe (9.34%), and Cl (0.73%).

4.2.1.1.3 Uranothorite [(Th, U) SiO_4]. Uranothorite can be found in the episyenite as anhedral to subhedral, rounded to subrounded grains with vitreous or resinous lustre and colours ranging from yellowish brown to dark yellow-brown. A combination of a binocular microscope (BSE), and (SEM/EDX) analysis of uranothorite mineral are shown in (Figure 6C). The EDS analysis data of uranothorite indicates that it contains U (19.36%), Si (16.22%), Al (2.85%), Th (49.08%), Y (6.41%), Ca (1.08%), and Fe (4.99%).

4.2.1.2 U-Phosphate

4.2.1.2.1 Autunite Ca [(UO_2) (PO_4)]$_2$ (H_2O)$_{11}$. Autunite is a typical uranyl mineral that can be found in oxidized uranium deposits, subsurface conditions that have been contaminated with uranium, and occasionally because of an alteration of uraninite or pitchblende. Important autunite minerals are distinguished by their limited solubility, which in large part regulates the mobility of uranium in the subsurface. Autunite is transparent to translucent with various colours such as Sulfur yellow to lemon yellow, greenish-yellow to pale green, and a Mohs scale hardness of 2–2.5 with a vitreous lustre. The backscattered image (BSE)/EDS) (Figure 6D) and the EDX analysis data of autunite show that it contains U (62.54%), Si (12.15%), Ca (6.85%), Al (9.95%), P (5.56%), Fe (1.85%), and k (1.10%).

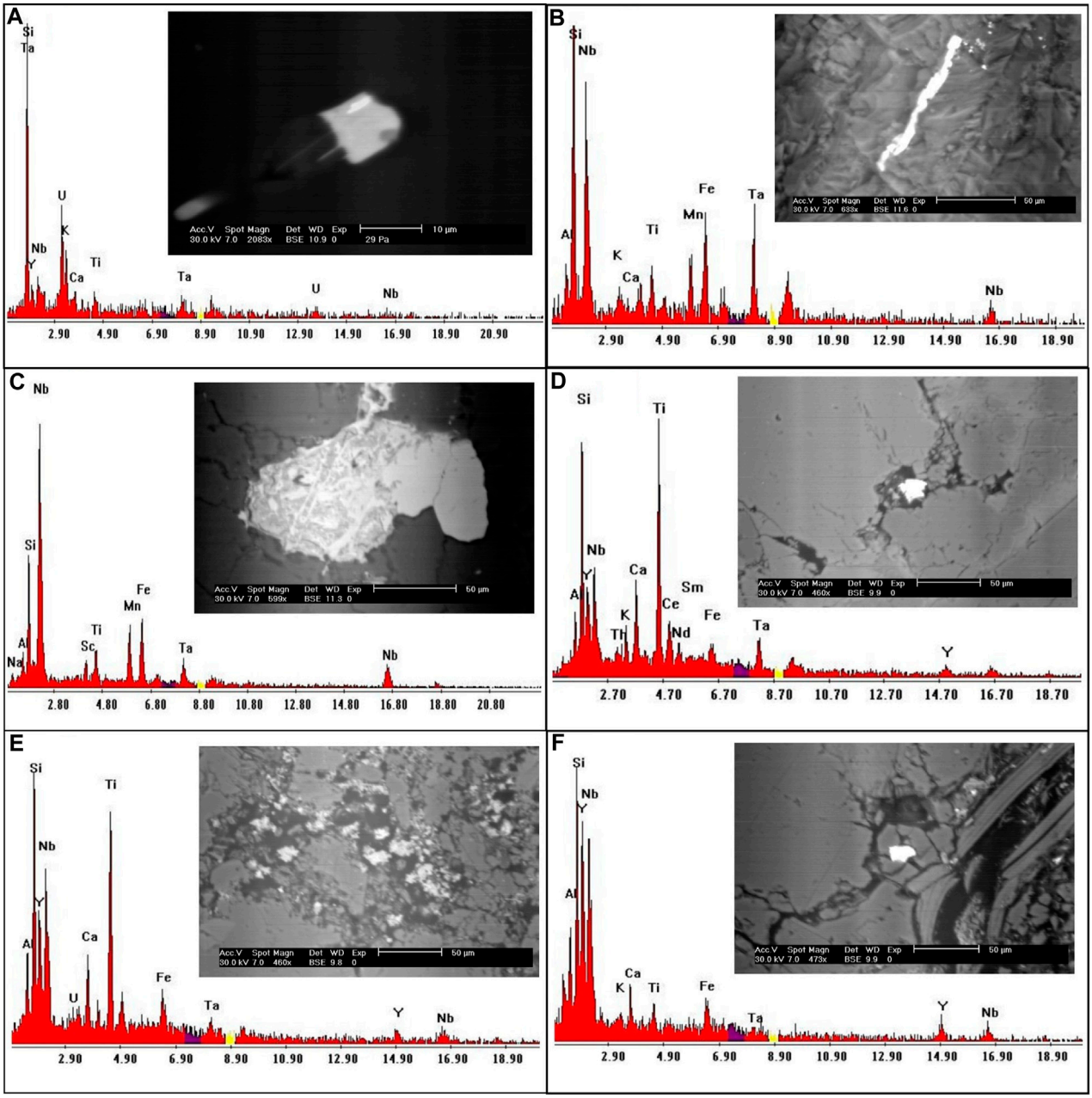

FIGURE 7
EDS analysis and BSE images for **(A)** Tapiolite mineral; **(B, C)** Columbite mineral; **(D, E)** Polycrase minerals; **(F)** Fergusonite mineral.

4.2.2 Radio and rare earth bearing minerals

4.2.2.1 Monazite [(Ce, La, Th, Nd, Y) PO_4]

Monazite can be found in the study area in a variety of shapes from spherical to oval, with colours ranging from yellowish to generally pale and lusters resinous, waxy, and vitreous. Monazite crystallizes in the monoclinic system and has 5–5.5 hardness on the Moho's scale. Using a binocular microscope, (SEM/EDX) and (BSE) analyses of monazite minerals are shown in (Figure 6E). The results of the EDX investigation show that there is Si (9.50 Wt. %), Al (3.90 Wt. %), P (14.24 Wt. %), U (3.76 Wt. %), Th (16.13 Wt. %) Ca (1.57 Wt. %), Fe (0.38 Wt. %), La (11.38 Wt. %), Ce (21.95 Wt. %), Pr (3.02 Wt. %), Nd (10.57 Wt. %), Sm (2.26 Wt. %) and Gd (1.32 Wt. %).

4.2.2.2 Xenotime (YPO_4)

Xenotime is a rare earth element (REEs) orthophosphate mineral, is the most abundant phosphorous-bearing mineral containing large amounts of heavy rare-earth elements (HREE) and occurs as an accessory mineral in rhyolites, pegmatites, metapelites and granitic rocks. Xenotime in the studied rock occurs in larger forms as anhedral aggregates, granular grains of dark brown to reddish-brown colour. Figure 6F shows a binocular microscope, (SEM/EDS) and (BSE) analysis of xenotime minerals. EDS analysis of xenotime mineral grains indicates that they are comprised principally of Y (36.54 Wt. %), Ca (1.71 Wt. %), K (0.65 Wt. %), Si (6.85 Wt. %), Al (2.93 Wt. %), Fe (1.16 Wt. %), P

(13.9 Wt. %), U (5.65 Wt. %), Mn (5.43 Wt. %), Yb (3.87 Wt. %), Ce (1.82 Wt. %), Dy (4.49 Wt. %), Er (3.02 Wt. %), Pr (6.76 Wt. %) and Nd (0.55 Wt. %).

4.2.3 Nb-Ta minerals

4.2.3.1 Tapiolite (Fe^{++}, Mn^{++}) $(Ta,Nb)_2O_6$

It is a dark mineral series that contains tantalum and niobium ore. Columbite and tantalite are quite close to tapiolite. These minerals have the same chemical makeup but differing crystal symmetry—tetragonal for tapiolite and orthorhombic for tantalite or columbite. In the research location, the tapiolite mineral was discovered and verified by ESEM (Figure 7A).

4.2.3.2 Columbite [(Fe, Mn, Mg) (Nb, Ta) $_2O_6$]

When the Nb/Ta ratios are 11.5 or greater, columbite and tantalite grade into one another (Tischendorf, 1977). According to the EDX studies, columbite is mostly made up of Nb (53.8 wt%) and Ta (11.5 wt%), with minor amounts of Fe and Mn (Figures 7B,C).

4.2.3.3 Polycrase-(Y) (Y,Ca, U, Th) $(Ti, Nb, Ta)_2O_6$

It belongs to the euxenite group and is radioactive because of the 6% or so uranium it contains. Polycrase forms a continuous series with the niobium-rich rare earth oxide euxenite. The ESEM analysis of the polycrase mineral is displayed in Figures 7D,E.

4.2.3.4 Fergusonite ($YNbO_4$)

Fergusonite is a significant species of minerals characterized by its unique chemical composition, which is generally represented as (Y, RE) NbO4. Here, 'Y' represents Yttrium, 'RE' signifies a spectrum of rare-earth elements, and 'NbO4′ denotes Niobium oxide. These rare-earth elements can form a solid solution with Yttrium, contributing to the mineral's complex constitution. As an accessory mineral, fergusonite is often found in granitic rocks, usually coexisting with one or more additional Yttrium, Thorium, Niobium, Tantalum, and Titanium oxide accessory minerals. This characteristic is widely acknowledged in the field of geological research (Lumpkin, 1998). Identification of fergusonite involves a detailed examination through an environmental scanning electron microscope (ESEM). Such analysis has revealed that the mineral has a Niobium content accounting for approximately 39 weight percent (wt.%) and Yttrium constituting around 26 wt%. Additionally, trace amounts of Iron are also detected in its composition, adding another dimension to its intricate chemical structure (as indicated in Figure 7F). In essence, the occurrence and identification of fergusonite in granitic rocks offer an intriguing study of the synergistic relationship between Yttrium, rare-earth elements, Niobium, and other mineral constituents. The mineral's composition underscores its complex formation processes and potential for various applications.

4.2.4 Accessory minerals

4.2.4.1 Beryl group

4.2.4.1.1 Bazzite [$Be_3(Sc, Al)_2Si_6O_{18}$]. In Baveno (Artini, 1915) first identified bazzite as a scandium silicate with an ambiguous chemical composition. Bazzite is the Sc analogue of beryl, according to research by (Bergerhoff and Nowacki, 1955; Peyronel, 1956)on the mineral from Val Strem (Grissona, Tavetsch, Switzerland) and Baveno, respectively. The bazzite mineral is registered for the first time in the mineral association of the studied area. Bazzite's chemical formula is $Be_3(Sc, Al)_2Si_6O_{18}$, an extremely rare Sc-bearing accessory mineral that is structurally similar to beryl (Figure 8A) (Peyronel, 1956) and containing around 50% of the octahedral positions inhabited by Sc^{3+} (Taran et al., 2017) Bazzite is the usual Fe^{2+} bearing silicates with Fe^{2+} in an octahedral structural position (Taran et al., 2017).

Generally, bazzzite is typically found as small to very small hexagonal crystals that are deep blue or blue-green in colour and difficult to tell apart from beryl. A binocular microscope study of the bazzite aggregate showed that most of the crystals are light blue, rounded to sub-rounded grains. There are two analyses by backscattered electron imaging (BSE), and a scanning electron microscope (SEM/EDX) (Figure 8B, C8), the first analysis is mainly composed of Sc (44.55 Wt. %), Si (33.43 Wt. %), Al (2.89 wt%), K (1.91 Wt. %), Ca (1.0 Wt. %), Mn (2.15 wt%), Fe (2.0 Wt. %), Ni (1.54 Wt. %) and Y (11.25 wt%). While the second analysis composed of Sc_2 (48.62 Wt. %), Si (32.61 Wt. %), P (2.55 wt %), Ca (1.20 Wt. %), Mn (1.98 wt%), Fe (2.83 Wt. %), Y (9.64 wt%) and Ni (1.46 Wt. %).

4.2.4.2 Zircon (ZrSiO4)

Zircon is metamict because it frequently has radioactive elements in its structure. Zr (44 weight percent), Hf (13.9 weight percent), and Si (31.2 weight percent) of Zircon were detected in the research region and confirmed by ESEM, with traces of U, Ca, and Al (Figure 8D).

4.2.4.3 Fluorite (CaF_2)

Fluorite is the mineral form of calcium fluoride (CaF_2) and is a significant host of fluorine. Fluorite is distinguished by various colours: yellowish brown, blue, pale rose, pale violet and dark violet with anhedral to subrounded, prismatic mineral grains, and vitreous luster with hardness 4 on the Moho's scale. The monazite mineral was examined using a combination of a binocular microscope, (SEM/EDS), and (BSE), as shown in (Figure 8E), EDS analyses demonstrate that it is constituted of F (16.70 Wt. %) and Ca (83.30 Wt. %).

4.2.4.4 Lead minerals

4.2.4.4.1 Cotunnite ($PbCl_2$). Cotunnite (lead chloride) $PbCl_2$ crystals are distinguished by orthorhombic symmetry, which accounts for the potential anisotropy of chloride ionic transport in these crystals. It occurs at temperatures below 325°C (Africano et al., 2002). Cotunnite in the studied area was found as anhedral to subhedral, rounded to subrounded grains of colourless to pale green, pale yellow, or light green with adamantine luster and white streak. Cotunnite crystals have 1½ - 2 ½ hardness on the Moho's scale. In (Figure 8F), cotunnite mineral analysis using a binocular microscope, (SEM/EDX), and (BSE) the EDX analysis of cotunnite mineral grains indicate that they are composed principally of Pb (65.33 Wt. %), Cl (26.32 Wt. %), Si (6.43 Wt. %), and Al (1.93 Wt. %).

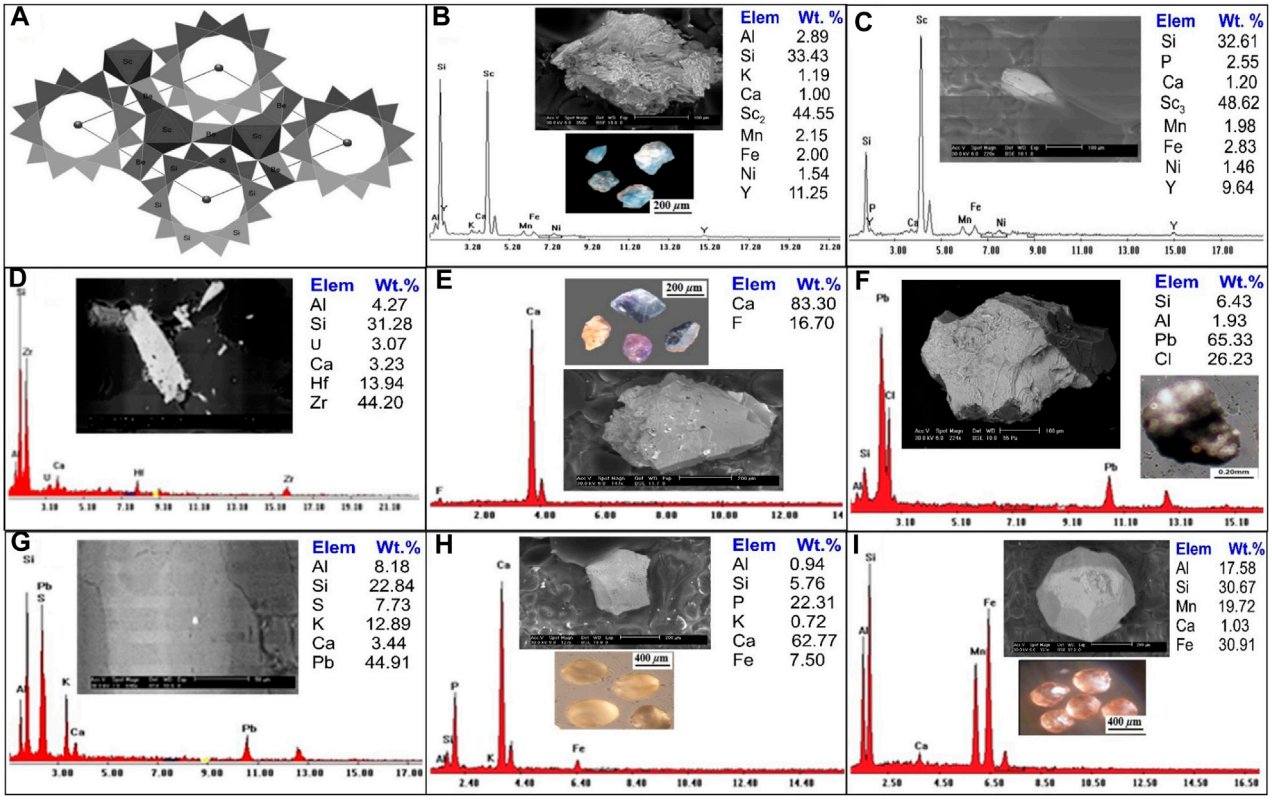

FIGURE 8
(A) General view of bazzite crystal fragments along the c-axis. (After Taran et al., 2017), Binocular microscope images, EDS analysis and BSE images for **(B, C)** Bazzite mineral; **(D)** Zircon mineral; **(E)** Fluorite mineral; **(F)** Cotunnite mineral; **(G)** Galena mineral; **(H)** Apatite mineral; **(I)** Garnets mineral.

4.2.4.4.2 Oxidized galena. The presence of galena, a lead grey mineral with a sub-metallic luster, has been noted in significant quantities. The occurrence of lead and zinc sulfide within this context could be attributed to either low-intermediate or high-temperature genesis, as described by (Howie et al., 1992). Energy-dispersive X-ray spectroscopy (EDX) analyses reveal that the primary constituents of galena are Lead (Pb) and Sulfur (S). Interestingly, this mineral is frequently found in association with, or as an inclusion within, potassium feldspar (k-feldspar). An intriguing observation from the EDX analysis is the relatively low concentration of Sulfur within the galena. This anomaly can be explained by prevailing oxidation conditions, which affect the overall composition of the mineral. These variations in the galena's composition, due to environmental factors, are visualized in Figure 8G. This in-depth analysis provides crucial insights into the galena's formation and its chemical properties, with implications for its potential applications and interactions with its surrounding environment.

4.2.5.5 Apatite $Ca_5(PO_4)_3(F,Cl,OH)$

The most prevalent phosphorus-bearing mineral is apatite, a frequent accessory mineral in many types of rocks. Weathering of apatite is the main source of phosphorus (P). Apatite occurs as white, brown to pale yellow, or reddish, rounded to subrounded grains that crystallize in the hexagonal system. The apatite mineral is investigated using a binocular microscope, (SEM/EDS) and (BSE) analysis are shown in (Figure 8H), EDX analysis of apatite mineral grains indicates that they are composed mainly of Ca (62.77 Wt. %), P (22.31 Wt. %), Si (5.76 Wt. %), Al (0.94 Wt. %), K (0.72 Wt. %) and Fe (7.50 Wt. %).

4.2.5.6 Garnet mineral [Almandine $Fe_3Al_2(SiO_4)_3$ and Spessartine $Mn_3Al_2(SiO_4)_3$) solid solution]

A garnet is a group of isomorphous minerals of different colours and compositions that characterize some igneous and metamorphic rocks and usually could be noticed as detritus grains in sediments. Garnet is distinguished by translucent grains of various colours, reddish-brown, brownish-yellow, and yellowish-green, with rounded to subrounded mineral grains. It has a vitreous luster, whereas the fracture luster is greasy, and has a hardness of 6.5–7.5 on the Moho's scale. A binocular microscope, (SEM/EDX) and (BSE) analysis of garnet mineral are shown in (Figure 8I). EDS analysis of garnet shows that it essentially contains Al (17.58 Wt. %), Si (30.67 Wt. %), Ca (1.03 Wt. %), Mn (19.72 Wt. %) and Fe (30.91 Wt. %).

4.3 Geochemistry of the episyenite rocks

The investigated area contains two varieties of episyenite, the first of which is the least desilicified and the other the most highly

10.3389/feart.2023.1241975

TABLE 2 Whole rock (Major oxides, trace and REE_S) of Kab Amiri episyenite, Central Eastern Desert, Egypt.

Rock type	Episyenite									
Petro. Name	Highly desilicified					Slightly desilicified				
S. No.	14 C	16 C	13 C	15 C	Av.	1 EP	2 EP	3 EP	4 EP	Av.
SiO_2	57.92	57.37	60.62	61.99	59.475	72.43	71.19	76.3	74.5	73.605
TiO_2	0.02	0.15	0.09	0.08	0.085	0.01	0.05	0.03	0.02	0.0275
Al_2O_3	16	12.94	13.2	15.48	14.405	14.79	13.84	11.89	13.1	13.405
FeO[t]	1.81	0.79	2.23	2.15	1.745	1.59	4.44	1.18	1.98	2.2975
MnO	0.35	0.17	0.32	0.03	0.2175	0.01	0.15	0.1	0.11	0.0925
MgO	0.45	0.02	0.38	0.22	0.2675	0.28	0.2	0.24	0.28	0.25
CaO	1.64	3.11	4.61	0.53	2.4725	1.56	1.12	1.62	1.56	1.465
Na_2O	10.54	9.5	4.58	6.02	7.66	3.76	4.01	3.44	3.64	3.7125
K_2O	5.72	6.99	6.36	6.91	6.495	3.64	3.2	3.96	3.37	3.5425
P_2O_5	0.01	0.03	0.03	0.03	0.025	0.23	0.2	0.03	0.02	0.12
L.O.I	5.34	7.5	6.18	5.56	6.145	0.7	0.8	0.9	0.78	0.795
total	99.8	98.57	98.6	99	98.99	99	99.2	99.69	99.36	99.31
Mo	101.28	4.24	30.6	1.6	34.43	3.2	4.6	8.5	4.9	5.3
Cu	2.5	4.8	15.6	77.8	25.16	10	8	8	6	8
Pb	16.82	15.35	9.7	31.53	18.35	16	11	10	19	14
Zn	212.7	25.5	89.1	33.9	90.3	24	26	36	33	29.75
Ag	20	31	51.8	343	111.45	20	35	20	49	31
Ni	0.6	1	4.3	5.7	2.9	15	7	6	66	23.5
Co	1	1	1.1	2	1.28	0.7	0.9	1.1	1	0.93
U	16.1	10.7	12.5	5.7	11.25	21.3	14.6	11.6	7.6	13.78
Th	24.6	11.6	20.9	5.5	15.65	33.6	20.3	18.6	9.6	20.53
Sr	33	81	57.9	48	54.98	294	122	128	98	160.5
V	99	9	63.7	10	45.43	20	15	25	19	19.75
Cr	2	1	5.2	60	17.05	9	9	8	7	8.25
Ba	62	103	80	112	89.25	100	14	145	138	99.25
Zr	62.9	44.6	40.8	36.9	46.3	574	243	251	315	345.75
Sn	324.2	20.6	89.7	6.1	110.15	32.2	45.3	75.3	21	43.45
Y	126.9	36.3	100.9	9.3	68.35	123	54	55	87	79.75
Hf	11.09	1.1	9.7	8.48	7.59	7.5	11.6	10.9	8.7	9.68
Rb	1395.1	261.7	589.3	738.7	746.2	970	948	190	235	585.75
Ta	51.1	31.9	45.1	55.1	45.8	29.6	35.6	42.14	17.9	31.31
Nb	173.59	49.66	75.5	49.95	87.18	116	49	85	135	96.25
Li	43.7	2	45.2	4.5	23.85	53	43.5	4.9	6.2	26.9
Cs	12.8	1.4	2.9	2.8	4.98	3.6	2.5	1.9	4.1	3.03
Ga	100	30.16	86.3	64.43	70.22	80	62.8	25.9	46.2	53.73
Sc	242	76.9	65.8	24.9	102.4	112	95	29.6	66	75.65

(Continued on following page)

TABLE 2 (*Continued*) Whole rock (Major oxides, trace and REE_S) of Kab Amiri episyenite, Central Eastern Desert, Egypt.

Rock type	Episyenite									
Petro. Name	Highly desilicified					Slightly desilicified				
S. No.	14 C	16 C	13 C	15 C	Av.	1 EP	2 EP	3 EP	4 EP	Av.
W	18.9	1.6	11.2	0.8	8.13	1.3	1.8	2.9	5.6	2.9
As	2.4	1.1	1.3	21	6.45	2.6	1.9	2.6	25	8.03
Sb	0.07	0.15	0.16	0.09	0.12	0.05	0.09	0.08	0.04	0.07
Bi	1.84	3.11	3.2	0.82	2.24	1.6	1.8	1.9	1.2	1.67
S	0.45	0.1	0.1	0.1	0.19	0.1	0.15	0.1	0.1	0.11
In	4.93	0.32	0.96	1.6	1.95	2.3	0.85	1.3	0.89	1.34
Re	0.002	0.002	0.002	0.002	0.002	0.002	0.002	0.002	0.002	0.002
Se	0.5	0.3	0.4	0.3	0.38	0.4	0.5	0.3	0.5	0.43
Te	0.91	1.55	1	1.23	1.17	1.1	0.87	1.66	2.1	1.43
Tl	4.48	1.74	7.2	4.32	4.44	3.9	2.6	5.7	3.6	3.95
La	2	11.6	6.9	7.4	6.98	4.5	1.3	9	6.3	5.28
Ce	13.53	24	20.3	20.74	19.64	18.6	12.5	32.2	16.3	19.9
Pr	3.8	5.4	5.6	3.6	4.6	3.6	1.9	4.9	4.2	3.65
Nd	19.4	17.9	20.1	9.7	16.78	9.9	7.6	17.9	12.6	12
Sm	10	5.4	9.5	2.6	6.88	4.3	4.9	7.5	4	5.18
Eu	0.1	0.1	0.2	0.2	0.15	0.5	0.4	0.5	0.5	0.48
Gd	10.9	3.9	10.2	1.8	6.7	2.8	2.2	4.3	3.5	3.2
Tb	2.8	0.9	2	0.3	1.5	0.4	0.5	0.7	0.8	0.6
Dy	16.7	5.3	10.9	1.8	8.68	3.5	4.3	4.8	4.4	4.25
Ho	3.7	1.2	2.5	0.3	1.93	0.7	0.9	0.8	0.9	0.83
Er	10.6	3.6	8	1.1	5.83	2.8	1.8	2.5	2.9	2.5
Tm	2.1	0.8	1.9	0.1	1.23	0.5	0.3	0.4	0.5	0.43
Yb	14.6	5.9	10.6	0.9	8	5.2	4.17	3.3	5.1	4.44
Lu	2.4	1.1	2.1	0.1	1.43	0.9	0.39	0.4	0.7	0.6
La/Nb	0.01	0.23	0.09	0.15	0.12	0.04	0.03	0.11	0.05	0.06
La/Ta	0.04	0.36	0.15	0.13	0.17	0.15	0.04	0.21	0.35	0.19
La/Lu	0.83	10.55	3.29	74	22.17	5	3.33	22.5	9	9.96
La/Y	0.02	0.32	0.07	0.8	0.3	0.04	0.02	0.16	0.07	0.07
Sr/Eu	330	810	289.5	240	417.38	588	305	256	196	336.25
Eu/Sm	0.01	0.02	0.02	0.08	0.03	0.12	0.08	0.07	0.13	0.1
Y/Ho	34.3	30.25	40.36	31	33.98	175.71	60	68.75	96.67	100.28
Zr/Hf	5.67	40.55	4.21	4.35	13.7	76.53	20.95	23.03	36.21	39.18
Nb/Ta	3.4	1.56	1.67	0.91	1.89	3.92	1.38	2.02	7.54	3.72
U/Th	0.65	0.92	0.6	1.04	0.8	0.63	0.72	0.62	0.79	0.69
Th/U	1.53	1.08	1.67	0.96	1.31	1.58	1.39	1.6	1.26	1.46
Ba/Sr	1.88	1.27	1.38	2.33	1.72	0.34	0.11	1.13	1.41	0.75

(Continued on following page)

10.3389/feart.2023.1241975

TABLE 2 (*Continued*) Whole rock (Major oxides, trace and REE_S) of Kab Amiri episyenite, Central Eastern Desert, Egypt.

Rock type	Episyenite									
Petro. Name	Highly desilicified					Slightly desilicified				
S. No.	14 C	16 C	13 C	15 C	Av.	1 EP	2 EP	3 EP	4 EP	Av.
Ba/Rb	0.04	0.39	0.14	0.15	0.18	0.1	0.01	0.76	0.59	0.37
Rb/Sr	42.28	3.23	10.18	15.39	17.77	3.3	7.77	1.48	2.4	3.74
ΣREE	112.63	87.1	110.8	50.64	90.29	58.2	43.16	89.2	62.7	63.32
LREE	48.83	64.4	62.6	44.24	55.02	41.4	28.6	72	43.9	46.48
HREE	63.8	22.7	48.2	6.4	35.28	16.8	14.56	17.2	18.8	16.84
LREE/HREE	0.77	2.84	1.3	6.91	2.96	2.46	1.96	4.19	2.34	2.74
Eu/Eu*	0	0.1	0.1	0.3	0.13	0.4	0.3	0.2	0.4	0.33
La/Yb_N	0.1	1.3	0.4	1.6	0.85	0.6	0.2	1.8	1.2	0.95
Tb/Yb_N	0.8	0.7	0.8	1	0.83	0.3	0.5	0.9	1.2	0.73
Gd/Yb_N	0.6	0.5	0.8	1.1	0.75	0.4	0.4	1.1	0.9	0.7
La/Sm_N	0.1	1.4	0.5	0.8	0.7	0.7	0.2	0.8	0.9	0.65
Ce/Ce*	1.516	0.856	0.985	1.224	1.15	1.519	2.552	1.36	0.982	1.6
t1	1.624	1.115	1.277	1.439	1.36	1.73	2.187	1.396	1.31	1.66
t3	1.171	1.098	1.005	1.087	1.09	0.919	1.133	1.075	1.149	1.07
TE1.3	1.379	1.106	1.133	1.251	1.22	1.261	1.574	1.225	1.227	1.32
t4	1.138	1.008	1.037	1.023	1.05	1.053	1.306	1.182	1.077	1.15
TE1,4	1.359	1.06	1.151	1.213	1.2	1.349	1.69	1.285	1.188	1.38

desilicified (Table 2). The sheared and hydrothermally altered portions of the primary pluton of post-orogenic granites, particularly near the contact with metasediments rock, are representative of the least desilicified episyenite. The separate small stock-like episyenite body that intrudes metasediments from the other side is associated with the highly desilicified granites (episyenite).

4.3.1 Major oxides

Values for major oxides in the two varieties of Kab Amiri epiyenitis are listed in table (2). The mean SiO_2 content was within the range of (57.37–61.99 wt.%) and (71.19–77.10 wt.%) in the highly and slightly desilicified episyenite samples, respectively. These values are shifted from the average of Kab Amiri fresh granite (77.12 wt.%), (Mahdy and El-Kammar, 2003). Al_2O_3 and FeO^t in the highly desilicified vary from 12.94 to 16.48 wt.% (average 15.06 wt.%), from 0.79 to 2.23 wt.% (average of 1.75 wt.%), respectively but in the slightly desilicified episyenite samples from 11.89 to 15.79 wt.% (mean 13.91 wt.%) and 1.18–4.44 wt.% (average 2.30 wt.%), respectively. The mean TiO_2 content is very low and varies from 0.02–0.15 wt.% and 0.01–0.05 wt.% in the highly and slightly desilicified episyenite, respectively.

CaO, Na_2O, MgO, and K_2O in the highly desilicified episyenite contents ranges are 0.53–4.61 wt.%, 4.58–10.54 wt.%, 0.02–0.45 wt.% and 5.72–6.99 wt.%, respectively. MnO and P_2O_5 concentrations in the highly and slightly desilicified episyenite samples are low and range from 0.03 to 0.35 wt%, 0.01–0.15 wt%, and 0.01–0.03 wt%, 0.02–0.23 wt%, respectively. L.O.I values are very low in the slightly desilicified episyenite in comparison with the highly desilicified episyenite.

5 Discussion

5.1 Depletion enrichment of major oxides, trace and (REE_S) in the highly and slightly desilicified episyenite

It is advised to normalise the altered rocks to the constant fresh granite of (Mahdy and El-Kammar, 2003) in order to better comprehend the elements' geochemical behaviour in the two episyenitized types. The reference granite then becomes flat at unity, and the deviations on either side of the reference line indicate whether the relationship is one of enrichment or depletion (Figure 9A, B). The geochemistry of major oxide is discussed in terms of gains (+ve) and losses (-ve) of these elements during the alteration of granites. The highly desilicified episyenite samples are affected by high desilicification and hematitization, which show increases in MgO, FeO^t, Al_2O_3, Na_2O, CaO, K_2O, TiO_2, P_2O_5 and MnO and deficiency in SiO_2. Enrichment of FeO^t may be resulted from the alteration of biotite (hematitization and chloritization). The increase of TiO_2 is mainly related to the occurrence of ilmenite and titanite. The increments in CaO can also

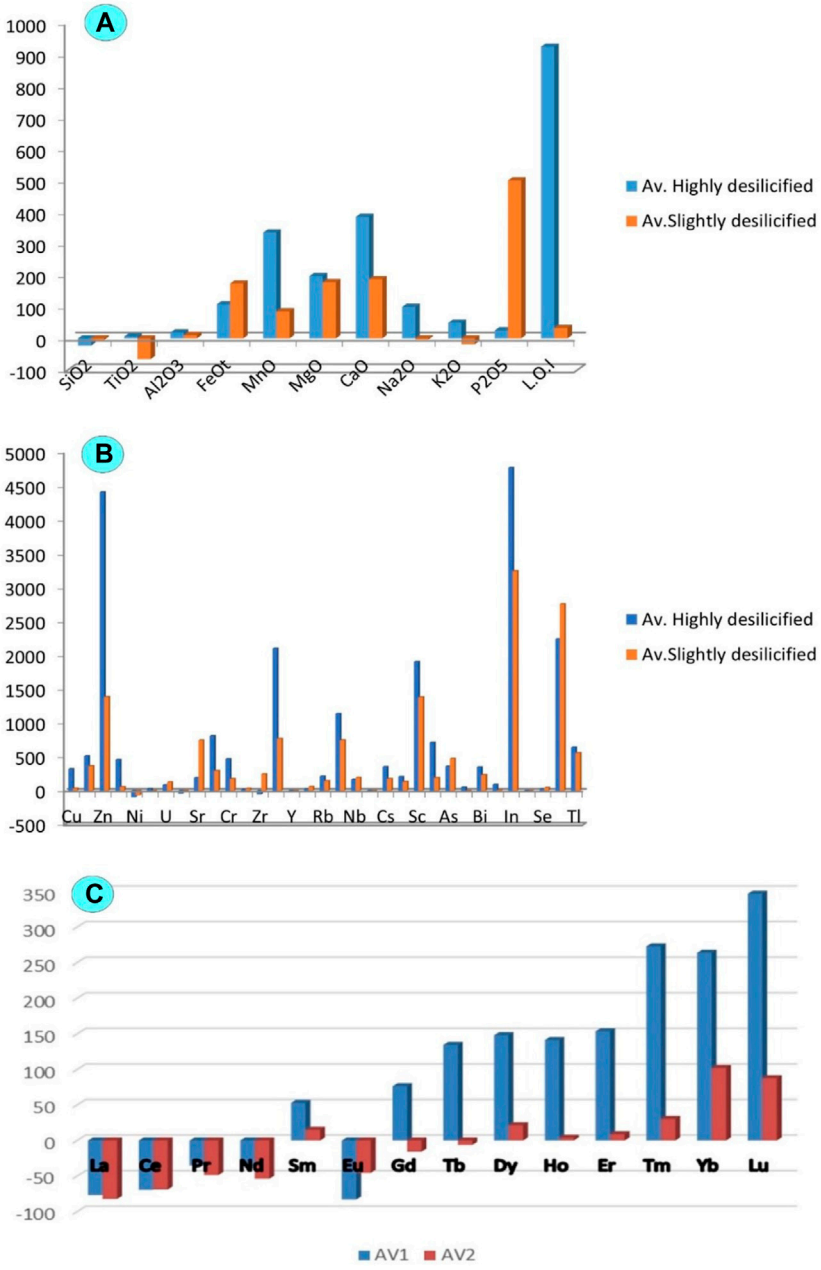

FIGURE 9
Histogram showing the depletion and enrichment for the least and highly desilicified episyenite **(A)** Major oxides; **(B)** Trace elements and **(C)** Rare earth elements.

be attributed to the occurrence of fluorite and calcite. Al_2O_3 enrichment might be associated with the alteration of k-feldspars (desilicification and sericitization). Quartz appears to have been dissolved by alkaline fluid (Figure 10A), leading to silica deficiency (El Feky et al., 2011). The enrichment in P_2O_5 may be influenced by the probable dissolution of monazite and xenotime, which was also noticed by (Cathelineau, 1987; El Feky et al., 2011).

Rezaei Azizi et al. (2017) pointed out the importance of trace elements such as Ta, Zr, Y, Nb, and REEs in various rock types and environments for deposit geochemistry and earth evolution. Most trace elements may be mobilised, and new mineral phases may form when minerals dissolve during hydrothermal alteration (El-Mezayen et al., 2015). Trace elements are enriched in Cu, Zn, U, Sr, Cr, Rb, Nb, Cs, Sc, As, Bi, In, Se, and Tl, while decreased in Ni, Zr, Y, and Th in the highly desilicified episyenite samples (Figure 9B). Furthermore, REEs in the highly desilicified samples show enrichment in (Sm, Gd, Tb, Dy, Ho, Er, Tm, Yb and Lu) whereas they are depleted in (La, Ce, Nd, Pr, Yb, and Eu), (Figure 9C). Rb increases with increasing sericite and K-feldspar. Only an increase in Sr resulted in Na-metasomatism.

Furthermore, the least altered episyenite shows an increase in FeO^t, Al_2O_3, MgO, CaO, MnO, and P_2O_5 and depletion in SiO_2, TiO_2, Na_2O, and K_2O (Figure 9A). The enhanced CaO contents may result from the

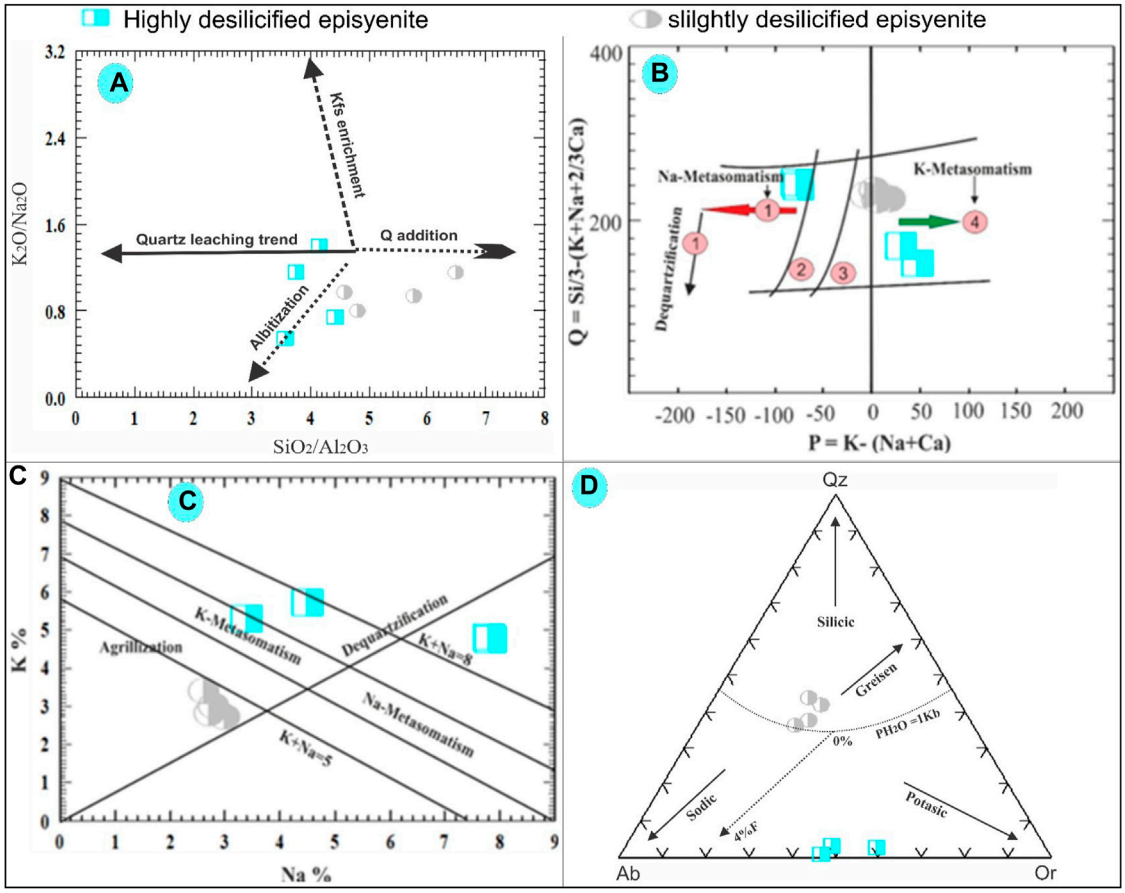

FIGURE 10
(A) K_2O/Na_2O *versus* SiO_2/Al_2O_3 binary diagram plots for the studied episyenite (Recio et al., 1997). **(B)** Q-P binary diagram of Cuney and Friedrich (1987). **(C)** Na-K binary diagram of Cuney and Friedrich. (1987). **(D)** Ab-Qz-Or normative diagram for the studied episyenite (Stemprok, 1979).

carbonization processes as indicated by the presence of calcite. The high FeO^t and MnO could be connected to the hematitization with solutions enriched in Iron and manganese. The enrichment of Al_2O_3 could result from the alteration of k-feldspars (kaolinization) and desilicification. The occurrence of xenotime, apatite and monazite may control enhancement in P_2O_5. The slightly episyenitized granite trace elements show enrichment in Cu, Sn, Nb, Ba, Rb, Mo, U, V, Ta, Sr, Hf, Pb, Zr, Ba and Zn whereas they are depleted in Ni and Y and in most LREEs (Figures 9B, C9).

5.2 Significance of the chemical characteristics and alteration stages of the episyenite

High silica depletion, typically followed by an increase in the other elements, is one of the most remarkable characteristics of episyenites compared to the unaltered granites. Simple quartz leaching could be the main reason for this enrichment (El Feky et al., 2011; El Gharbawy and El Maadawy, 2012). stated that the granitic rocks are generally altered after solidification and emplacement due to the effect of residual solutions, which are rich in water, causing deuteric and hydrothermal alteration processes. The fresh granites of the Kab Amiri area were subjected to two phases of desilicifications; the first was weak, leading to slight silica deficiency, while the latter was very strong, resulting in high silica deficiency, forming the spongy nature of episyenite.

According to the K_2O/Na_2O *versus* SiO_2/Al_2O_3 diagram of (Recio et al., 1997), because of the addition of either albite or K-feldspar, most of the highly and slightly desilicified episyenite samples show the probable evolutionary trend followed by the albitization. However, the changes in Si and alkali could be explained by the interaction of quartz and the addition of albite and quartz to varying degrees (Figure 10A). Plotting the slightly and highly desilicified episyenite on the Q-P diagram of (Cuney and Friedrich 1987) clarifies that the highly desilicified samples suffered from Na- and K-metasomatism with dequartzification, while the slightly altered episyenite samples show the effect of incipient dequartzification with K-metasomatism (Figure 10B). In order to distinguish between distinct alteration zones, such as argillic, potassic, sodic, and dequartzification modifications (Cuney and Friedrich 1987), created a Na-K diagram (Figure 8C). The area of the diagram on the left, where K increases and Na decreases, is the only region where K-metasomatism occurs. The Na-metasomatism field, where Na increases, and K decreases, is shown on the right side of the diagram. The argillic field was limited to the lower half of the

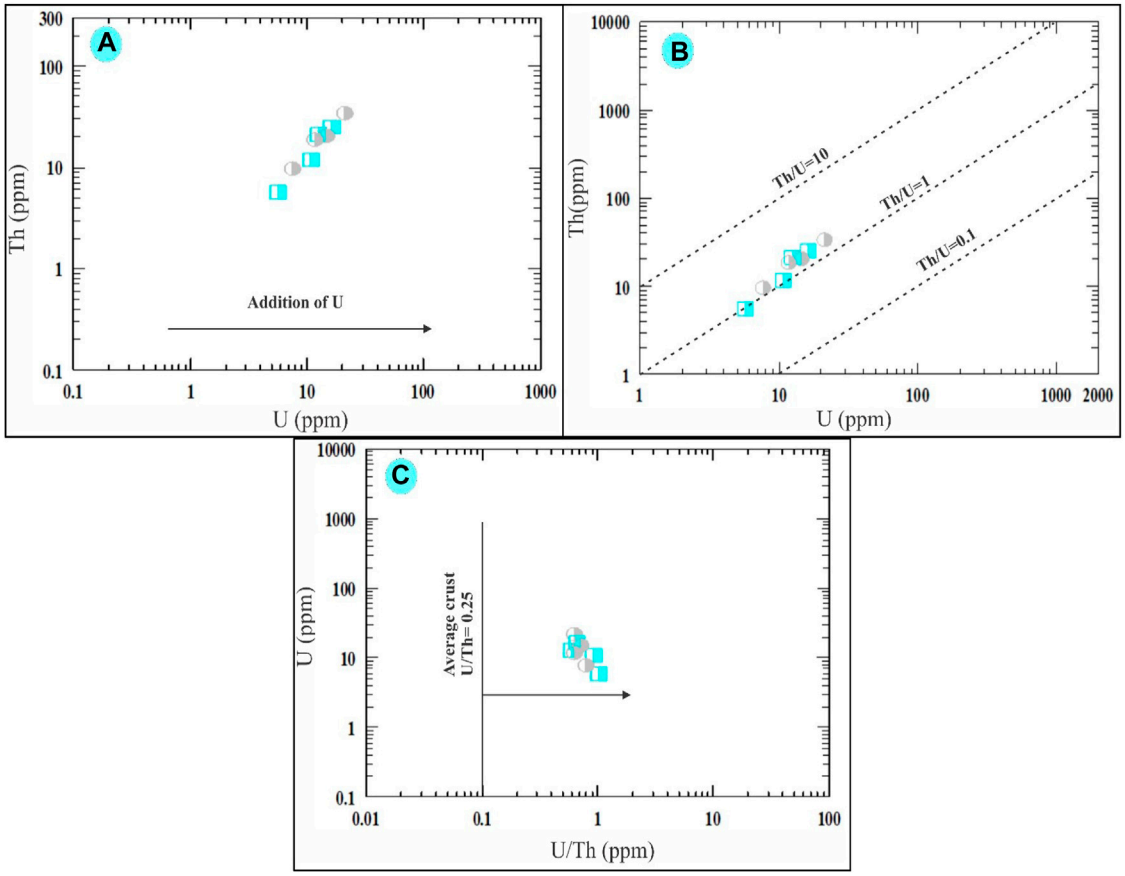

FIGURE 11
Binary diagrams showing. Th vs. U variation diagram of **(A)** Alexandre (2010) and **(B)** Cuney et al. (2012). **(C)** U vs. U/Th plot showing the enrichment of uranium in the episyenite (Mason and Moore, 1991). The same symbols used in (Figure 10).

Na-K binary diagram, which showed that altered rocks were subject to high Na and K leaching conditions. While highly desilicified episyenite samples are found close to the argillic alteration zone, samples of strongly desilicified episyenite are found in the sodic and potassic sectors. According to (Stemprok, 1979), normative Ab-Qz-Or ternary diagram composition can be divided into four categories: greisen, silicic and potassic. The studied slightly desilicified episyenite samples contain a high SiO_2 content and follow the trend of greizenization while the highly desilicified episyenite samples have low SiO_2, Na, and K contents, so they shifted towards sodic and potassic trends (Figure 10D).

5.3 Geochemistry of isovalents

According to (Dostal and Chatterjee, 2000), Zr/Hf ratios have a limited range of 33–40, with an average of 34.2 ± 0.3. Divergence from the range was uncommon and usually brought on by significant fractionation of auxiliary minerals or metasomatism. According to (Irber, 1999; Khamis et al., 2020), the majority of the highly desilicified episyenite samples show decreased Zr/Hf ratios and move towards smaller values (20). This indicates that these rocks were affected by severe magmatic-hydrothermal alteration in highly fractionated silicate melt. In contrast, the Zr/Hf ratio values of the majority of slightly desilicified episyenite samples are higher than the chondritic ratio values, suggesting that this alteration phase could result from the effect of low-temperature F-rich solution as clarified by (Firdaus et al., 2011). Higher than chondritic and lower Zr/Hf ratio values in the highly and slightly desilicified episyenite samples, respectively, could be related to the traditional contact between the two phases and field relation difficulties to separate them. The Y/Ho ratio (Y/Ho = 28.8) deviates from the chondritic value (Zhang et al., 1994; Bau, 1996). Highly desilicified episyenite samples have a Y/Ho value slightly higher than the chondritic value. In comparison, the value in slightly desilicified episyenite samples is significantly greater than the chondritic values, indicating that these rocks have undergone different stages of hydrothermal alteration with fluorine or bicarbonate, as shown by the mineralogical analyses. Nb/Ta ratios of the investigated highly and slightly desilicified episyenite are non-chondritic (0.91–3.40 for highly desilicified and 1.38–7.54 for slightly desilicified episyenite). Ratios of La/Nb and La/Ta are (0.01–0.23 and 0.03–0.11), (0.04–0.36 and 0.04–0.35) for highly desilicified and slightly desilicified episyenite, respectively. Nb/Ta has a chondritic ratio of 17.6 ± 1, (0.96–1) for La/Nb and (16–18) for La/Ta (Jahn et al., 2001). They are thought to be substantially distinct, according to these non-chondritic ratios.

U-rich metamorphic and possibly granitic rocks are considered the source of uranium in epiyenites, and it is generally accepted that U is mobile predominantly in oxidised fluids. In general, granite fertility denotes the presence of leachable uranium oxide and a whole-rock uranium level of greater than 10 ppm (Tartèse et al., 2013), upper crust value for the U (2.7 ppm) (Rudnick et al., 2003); and in comparison to the crustal levels of 1.8 ppm.

The study reveals interesting findings about uranium (U) and thorium (Th) concentration in the episyenite samples (Mason, 1952). point out that the average content of U is 2.6 ppm, and Th is 7.2 ppm in a typical upper crust. However, our analysis of the highly and slightly desilicified episyenite samples shows higher values. The average U content is found to be 11.25 ppm in the highly desilicified sample and 13.78 ppm in the slightly desilicified sample. For Th, the average content is 15.65 ppm and 20.53 ppm in the highly and slightly desilicified samples, respectively. Thus, both U and Th contents surpass the average upper crust values. Chemical analysis of the uranium and thorium content in these episyenite samples reveals a positive correlation, a finding in line with (Alexandre, 2010), suggesting a differentiation process and uranium enrichment (Figure 11A). This may be attributed to uranium leaching from metamictized U-bearing accessory minerals like allanite, Zircon, and monazite, or major minerals such as muscovite during episyenitization, leading to additional uranium content (López-Moro et al., 2019). Regarding the Th/U ratio, the values for both the highly and slightly desilicified samples (average 1.31 and 1.46 ppm, respectively) are substantially lower than the average continental crust value of 3.80 ppm (Van Schmus, 2013). This decrease in the Th/U ratio suggests that the magma was deficient in accessory minerals due to the low content of rare earth elements (REEs). The Th *versus* U variation diagram by (Cuney et al., 2012) also illustrates a weak positive correlation between Th and U in the studied samples (Figure 11B). Lastly, the U/Th ratio (average 0.80 and 0.69 ppm for the highly and slightly desilicified samples, respectively) is significantly higher than the average continental crust value of 0.25 ppm (Mason, 1952). This implies an increase in these elements within the episyenite rocks (Figure 11C).

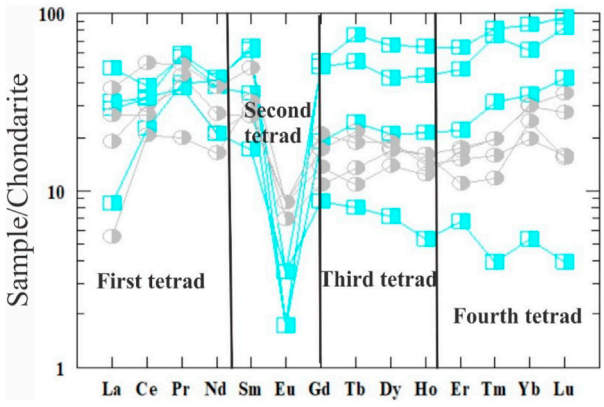

FIGURE 12
Chondrite normalized REEs diagram (Boynton, 1984) of the studied episyenite. The same symbols used in (Figure 10).

5.4 Rare earth elements geochemistry

The mobility of REEs in the crust is largely determined by the character of their host minerals and the composition of the fluids involved in the water-rock interaction (Humphris, 1984). During the formation of the episyenite, the REEs may remain almost motionless. (Hecht et al., 1994).

The average ΣREE contents of the highly and slightly desilicified episyenite are 90.29 and 63.32 ppm, respectively (Table 2), but the average ΣLREE is 55.02 and 46.48 ppm is higher than the average ΣHREE 35.28 and 16.84 ppm in the highly desilicified and slightly desilicified episyenite respectively. The dissolution of monazite and potentially other LREEs-bearing minerals is most likely to be responsible for the LREEs depletion (e.g. fluocerite). The production

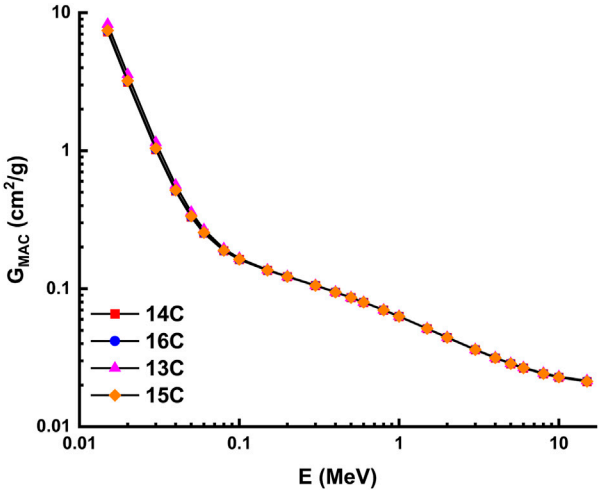

FIGURE 13
Variation of mass attenuation coefficient with photon energy for highly desilicified samples.

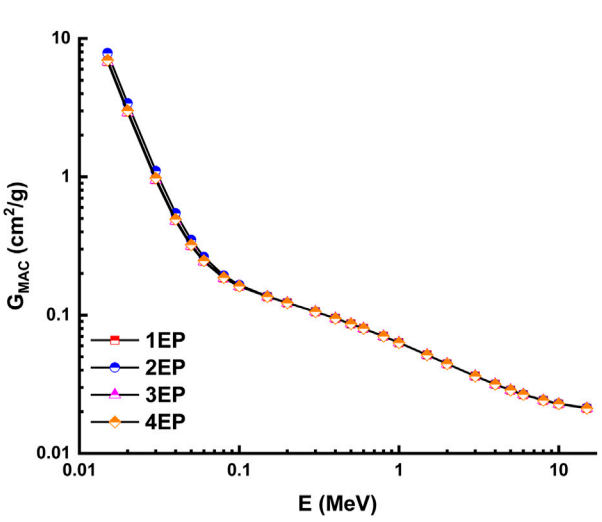

FIGURE 14
Variation of mass attenuation coefficient with photon energy for slightly desilicified samples.

of HREEs-bearing Nb-Ti-Y oxide minerals explains the HREEs enrichment in episyenite. The LREEs (La/Sm_n= 0.5–1.4 and 0.2–0.9) and the HREEs (Gd/Yb_n= 0.5–1.1 and 0.4–1.1) and negative Eu anomaly characterise where this granite was Eu/Eu* (0.1–0.3 and 0.2–0.4) in the highly and slightly desilicified episyenite respectively. The REEs content particularly that of the Kab Amiri episyenites, shows considerable REEs fractionation and mobility during hydrothermal alteration (Figure 12).

The metasomatized granites of Kab Amiri have strong convex (M-type) first tetrad (T_1), with values ranging between 1.12 and 1.62 in the highly desilicified, whereas between 1.31 ad 2.19 in the least desilisified graites. While the third and fourth segments (T_3 and T_4) are much less developed in the two types (Table 2; Figure 12). (Mahdy and El-Kammar, 2003) noted the presence of the W-type tetrad effect in some samples and mentioned that the alkali-metasomatism of the Kab Amiri granitoid occurred under physico-chemical conditions that were constantly changing; therefore the alteration products varied from one location to another. These phenomena confirm the presence of more than one stage of hydrothermal alteration (Taalab et al., 2023). There are two stages of hydrothermal alterations for the fresh Kab Amiri granites, causing mild epsyenitization at contact with the metasediments forming the least altered episyenitized granite and severe epsyenitization in the separated cone shape stock with the known spongy episyenite. The earliest hydrothermal fluids were accommodated by noticeable petrographical, chemical and mineralogical changes between the least and highly episyenitized granites. The least episyenitized granites have elevated amounts of Fe, P, Zr, Ni, U, Th, Ba, Y, Hf, Nb, and As, which are correlated with their mobilization from biotite, k-feldspar, plagioclase and metamict zircon. These elemental changes are related the partial albitization, muscovitization, desilicification and chloritizatiom, which lead to the mobilization of these elements and the forming of specific mineral associations in the least altered granites such as autonite,

TABLE 3 Mass attenuation coefficient of highly desilicified and slightly desilicified samples.

E (MeV)	Highly desilicified samples				Slightly desilicified samples			
	14C	16C	13C	15C	1EP	2EP	3EP	4EP
0.015	7.283	7.388	8.251	7.438	6.820	7.855	6.771	6.976
0.020	3.147	3.186	3.570	3.214	2.942	3.409	2.919	3.012
0.030	1.019	1.028	1.147	1.039	0.956	1.103	0.949	0.978
0.040	0.509	0.512	0.563	0.518	0.483	0.546	0.480	0.493
0.050	0.331	0.332	0.358	0.335	0.318	0.350	0.316	0.323
0.060	0.252	0.253	0.268	0.255	0.245	0.264	0.244	0.248
0.080	0.188	0.189	0.195	0.189	0.186	0.193	0.185	0.187
0.100	0.163	0.163	0.166	0.163	0.162	0.165	0.161	0.162
0.150	0.136	0.136	0.137	0.136	0.136	0.137	0.136	0.136
0.200	0.122	0.122	0.123	0.123	0.123	0.123	0.123	0.123
0.300	0.106	0.106	0.106	0.106	0.106	0.106	0.106	0.106
0.400	0.094	0.094	0.095	0.095	0.095	0.095	0.095	0.095
0.500	0.086	0.086	0.086	0.086	0.086	0.086	0.087	0.087
0.600	0.080	0.080	0.080	0.080	0.080	0.080	0.080	0.080
0.800	0.070	0.070	0.070	0.070	0.070	0.070	0.070	0.070
1.000	0.063	0.063	0.063	0.063	0.063	0.063	0.063	0.063
1.500	0.051	0.051	0.051	0.051	0.052	0.051	0.052	0.052
2.000	0.044	0.044	0.044	0.044	0.044	0.044	0.044	0.044
3.000	0.036	0.036	0.036	0.036	0.036	0.036	0.036	0.036
4.000	0.032	0.032	0.032	0.032	0.032	0.032	0.032	0.032
5.000	0.029	0.029	0.029	0.029	0.029	0.029	0.029	0.029
6.000	0.027	0.027	0.027	0.027	0.027	0.027	0.027	0.027
8.000	0.024	0.024	0.024	0.024	0.024	0.024	0.024	0.024
10.000	0.023	0.023	0.023	0.023	0.023	0.023	0.023	0.023
15.000	0.021	0.021	0.022	0.021	0.021	0.021	0.021	0.021

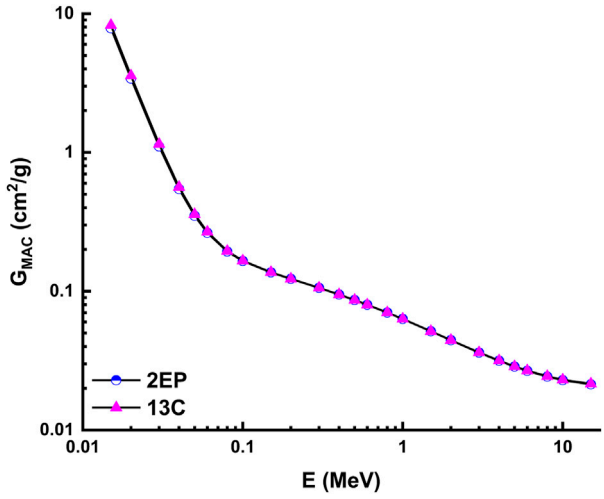

FIGURE 15
Variation of mass attenuation coefficient with photon energy for 2EP and 13C samples.

tripiolite, columbite, Zircon and galena. On the other hand, in the second stage, granites were subjected to intense alteration processes by mineralizing fluids causing wholly muscovitization of biotite and feldspar, albitization of plagioclase, carbonitization and apatitization. Many elements were mobilized from these altered minerals, including Ti, Al, Mn, Mg, Ca, Na, K, Mo, Cu, Pb, Zn, Ag, Co, Sr, V, Cr, Sn, Rb, Ta, Li, Sc, W, S, In, and Tl, leading to definite mineralization as kaslite, monazite, xenotime, polycrase and apatite. The mineralizing fluids in the least and highly episyenitized granites are incorporated in some ore minerals like uranophane, fergusonite, bazzite and garnet.

5.5 Radiation shielding characteristics

The theoretical calculations for the radiation shielding characteristics were performed using the NISTXCOM online across a range of energies extending from 0.015 to 15 MeV (Berger and Hubbell, 1987). The mass attenuation coefficient, also known as G_{MAC}, is shown in Figure 13 and Figure 14 for the highly desilicified (14C, 16C, 13C, and 15C) and the sightly desilicified (1EP, 2EP, 3EP, and 4EP) samples, respectively. In addition, the full results have been listed in Table 3. These graphs illustrate the inverse connection that exists between the amount of photon energy and the G_{MAC} values. A larger amount of photon energy will result in lower G_{MAC} values. This decrease results from various interactions between photons and matter, including photoelectric, Compton scattering, and pair creation, among others. 7.283, 7.388, 8.251, 7.438, 6.820, 7.855, 6.771, and 6.976 are G_{MAC} values for 14C, 16C, 13C, 15C,1EP, 2EP, 3EP, and 4EP at 15 keV. Among the highly desilicified samples, 13C has the highest G_{MAC} values. At the same time, 2EP sample has the highest G_{MAC} values among slightly desilicified samples. In addition, the 2EP sample has the highest G_{MAC} values compared to the values of all samples (Figure 15).

The unique geochemical and mineralogical characteristics of the Kab Amiri granites, especially their richness in heavy minerals and elements such as U, Th, and other rare earth elements (REEs), underline their potential as an innovative material for radiation shielding. Furthermore, our research on the various stages of episyenitization and the subsequent alteration processes not only delves into the geological significance of these granites but also emphasizes their practical relevance. Theoretical calculations using the NISTXCOM online, as highlighted in our results, demonstrate the potential of these granites in radiation shielding applications across a wide energy range. With the increasing demand for radiation shielding in various industries, such as nuclear energy, healthcare, and space exploration, the insights provided by our study can pave the way for exploring granitic rocks as alternative or enhanced shielding materials. Furthermore, our research has the potential to contribute significantly to radiation protection technology. The in-depth characterization of the least and most extensively desilicified episyenite can lead to the development of innovative techniques that optimize the properties of existing shielding materials, extending their lifespan, reducing cost, and enhancing radiation protection efficiency.

6 Conclusion

There is a clear increment in some major oxides, trace and REEs of the highly episyenitized granites and deficiency in the others concerning the least episyenitized granites (Table 1). The increase in Al_2O_3, CaO, Na_2O, K_2O, P_2O_5, L.O.I, Mo, Cu, Pb, Zn, Ag, V, Cr, Sn, Y, Ta, Nb, and REEs contents in the highly episyenitized granites in comparison with the least episyenitized granites, where they show a decrement in SiO_2, FeO^t, MnO, MgO, P_2O_5, Ni, U, Th, Sr, Ba, and Zr. High values of the loss of ignition (L.O.I.) in the study samples are mostly due to intergranular water saturation, hydrous mineral production (such as sericite and muscovite), and carbonate formation. The presence of calcite and fluorite can also be credited with the enrichment of CaO. The sericitization and desilicification of k-feldspars may be connected to the enrichment of Al_2O_3. The P_2O_5 increment may be controlled by the occurrence of apatite, xenotime, and monazite. The compositional discrepancies between the major ionic lithophile elements Sr, Ba, and Rb represent the degree of alteration present in the episyenite rock. Due to their extremely close ionic radii, Rb and Ba are frequently coupled with K+, and all of them can be found in muscovite and k-feldspar. The modest rise in Sr in episyenite can be explained by a higher concentration of (albites) and alkali feldspars. Tetrad effects in these rocks confirm the mobilisation of these elements. La/Y ratios less than unity show an acidic environment, whereas those more than unity show an alkalic environment. All samples of the highly and slightly episyenitized granites have La/Y ratios <1, indicating the prevailing acidic conditions in the depositional environment, especially in the highly episyenitized granites, suggesting very high acidic conditions leading to trace and REEs mobilization. The diminution of REEs contents could be attributed to their mobilization to the adjacent rocks. Zr/Hf, La/Y, Nb/Ta, Y/Ho, and Th/U ratios with pronounced tetrad effects in the two stages of episyenitization could be related to the Physico-chemical changes

associating hydrothermal and supergene alterations in the rock types leading to unusual mobilization of major, trace and rare earth elements. Notably, the Gross Mass Attenuation Coefficient (G_{MAC}) values derived from the samples indicate that the radiation shielding properties of these episyenitized granites are significant. Specifically, the highly desilicified sample 13C and slightly desilicified sample 2EP displayed the highest G_{MAC} values, thus suggesting their superior potential for radiation shielding applications. Exploring these rocks for such practical purposes can be a promising direction for future research.

Data availability statement

The original contributions presented in the study are included in the article/supplementary material, further inquiries can be directed to the corresponding authors.

Author contributions

Conceptualization, ST and HZ; methodology, ST and SI; software, ST and HA; validation, NA, and AA; formal analysis, AE, AA, HA, and AE; investigation, AE and NA; resources, ST; data curation, AE, AA, and SI; writing—original draft preparation, ST, HZ, AE, and SI; writing—review and editing, HA, AA, HZ, and NA; visualization, AE, and MR; supervision, HZ; funding acquisition, AE and AA. All authors contributed to the article and approved the submitted version.

Funding

The authors express their gratitude to Princess Nourah bint Abdulrahman University Researchers Supporting Project (Grant No. PNURSP2023R378), Princess Nourah bint Abdulrahman University, Riyadh, Saudi Arabia. The work of the author AE and APC was covered by "Dunarea de Jos" University of Galati, Romania.

Conflict of interest

The authors declare that the research was conducted in the absence of any commercial or financial relationships that could be construed as a potential conflict of interest.

Publisher's note

All claims expressed in this article are solely those of the authors and do not necessarily represent those of their affiliated organizations, or those of the publisher, the editors and the reviewers. Any product that may be evaluated in this article, or claim that may be made by its manufacturer, is not guaranteed or endorsed by the publisher.

References

Abd El Rahman, R. M., Taalab, S. A., Al Full, Z. Z., Mohamed, M. S., Sayyed, M. I., Almousa, N., et al. (2022). Natural radionuclide levels and radiological hazards of khour azalea mineralized pegmatites, southeastern desert, Egypt. *Minerals* 12, 353. doi:10.3390/min12030353

Abdel Meguid, A. A., Ammar, S. E., Ibrahim, T. M. M., Ali, K. G., Shahin, H. A., Omer, S. A., et al. (2003). *Uranium potential of Eastern Desert granites, Egypt*. Egypt: NMA internal report for project: EGY/03/014 technical Assistance by IAEA, 270.

Abdel-Rahman, A. M., El-Desoky, H. M., Shalaby, B. N. A., Awad, H. A., Ene, A., Heikal, M. A., et al. (2022). Ultramafic rocks and their alteration products from northwestern allaqi province, southeastern desert, Egypt: petrology, mineralogy, and geochemistry. *Front. Earth Sci.* 10, 894582. doi:10.3389/feart.2022.894582

Africano, F., Van Rompaey, G., Bernard, A., and Le Guern, F. (2002). Deposition of trace elements from high temperature gases of Satsuma-Iwojima volcano. *Earth, planets Sp.* 54, 275–286. doi:10.1186/bf03353027

Alexandre, P. (2010). Mineralogy and geochemistry of the sodium metasomatism-related uranium occurrence of Aricheng South, Guyana. *Min. Depos.* 45, 351–367. doi:10.1007/s00126-010-0278-7

Artini, E. (1915). Due minerali di Baveno contenenti terre rare: weibyeïte e bazzite. *Rendic. Acc. Lincei* 24, 313–319.

Awad, H. A., Abu El-Leil, I., Nastavkin, A. V., Tolba, A., Kamel, M., El-Wardany, R. M., et al. (2022a). Statistical analysis on the radiological assessment and geochemical studies of granite rocks in the north of Um Taghir area, Eastern Desert, Egypt. *Open Chem.* 20, 254–266. doi:10.1515/chem-2022-0131

Awad, H. A., El-Leil, I. A., Nastavkin, A. V., Tolba, A., Kamel, M., El-Wardany, R. M., et al. (2022b). Statistical analysis on the radiological assessment and geochemical studies of granite rocks in the north of Um Taghir area, Eastern Desert, Egypt. *Open Chem.* 20, 254–266. doi:10.1515/CHEM-2022-0131

Awad, H. A. M., Zakaly, H. M. H., Nastavkin, A. V., and El-Taher, A. (2020). Radioactive content and radiological implication in granitic rocks by geochemical data and radiophysical factors, Central Eastern Desert, Egypt. *Int. J. Environ. Anal. Chem.* 102, 7444–7457. doi:10.1080/03067319.2020.1830987

Bau, M. (1996). Controlsonthefractionationofisovalenttrace elementsinmagmaticand aqueoussystems: evidencefromY/Ho, Zr/Hf, andlanthanidetetradeffect. *Contrib. Mineral.* 123, 323–333. doi:10.1007/s004100050159

Berger, M. J., and Hubbell, J. H. (1987). *Xcom: Photon cross sections on a personal computer*. Oak Ridge, TN: Center for Radiation Research. doi:10.2172/6016002

Bergerhoff, G., and Nowacki, W. (1955). Über die Kristallstruktur des Bazzit und ihre Beziehungen zu der des Beryll. *Schweiz. Min. Petrogr. Mitt* 35, 410–421. doi:10.5169/seals-27856

Boynton, W. V. (1984). "Geochemistry of rare earth elements: Meteorite studies," in *Rare Earth Elements Geochemistry*. P. Henderson Amsterdam: Elsevier Pub. Co., 63–114.

Cathelineau, M. (1987). U-Th-REE mobility during albitization and quartz dissolution in granitoids: evidence from south-east French massif central. *Bull. Minéralogie* 110, 249–259. doi:10.3406/bulmi.1987.7984

Cuney, M., Emetz, A., Mercadier, J., Mykchaylov, V., Shunko, V., and Yuslenko, A. (2012). Uranium deposits associated with Na-metasomatism from central Ukraine: A review of some of the major deposits and genetic constraints. *Ore Geol. Rev.* 44, 82–106. doi:10.1016/j.oregeorev.2011.09.007

Cuney, M., and Friedrich, M. (1987). Physicochemical and crystal-chemical controls on accessory mineral paragenesis in granitoids: implications for uranium metallogenesis, Bull. *Minéral* 110, 235–247. doi:10.3406/bulmi.1987.7983

Dostal, J., and Chatterjee, A. K. (2000). Contrasting behaviour of Nb/Ta and Zr/Hf ratios in a peraluminous granitic pluton (Nova Scotia, Canada). *Chem. Geol.* 163, 207–218. doi:10.1016/s0009-2541(99)00113-8

El Bahariya, G. A. (2021). An overview on the classification and tectonic setting of neoproterozoic granites of the nubian Shield, Eastern Desert, Egypt. *Geochemistry*. doi:10.5772/intechopen.95904

El Feky, M. G., El Mowafy, A. A., and Abdel Warith, A. (2011). Mineralogy, geochemistry, radioactivity and environmental impacts of Gabal Marwa granites, southeastern Sinai, Egypt. *Chin. J. Geochem.* 30, 175–186. doi:10.1007/s11631-011-0499-1

El Gharbawy, R. I., and El Maadawy, W. M. (2012). Geochemistry of the uranium-thurium-bearing granitic rocks and pegmatites of Wadi Haleifiya area, Southeastern Sinai, Egypt. *Chin. J. Geochem.* 31, 242–259. doi:10.1007/s11631-012-0573-3

El Mezayen, A. M., Ibrahim, E. M., El-Feky, M. G., Omar, S. M., El-Shabasy, A. M., and Taalab, S. A. (2022). Physico-chemical conditions controlling the radionuclides mobilisation in various granitic environments. *Int. J. Environ. Anal. Chem.* 102, 970–986. doi:10.1080/03067319.2020.1729758

El-Desoky, H. M., Abdel-Rahman, A. M., Ene, A., Khalil, A. E., Fahmy, W., Zakaly, H. M. H., et al. (2022). Origin and heavy metals of plagio-granites in Egyptian Shield oceanic complexes: A case study of abu dabbab area, central Eastern Desert, Egypt. *Miner* 12, 1093. doi:10.3390/MIN12091093

El-Mezayen, A. M., El-Feky, M. G., Omar, S. A., and Ibrahim, S. A. (2015). Geochemistry and a composite M-type with W-type of REE tetrad effect in altered granites of Abu Furad area, Central Eastern Desert, Egypt. *Greener J. Geol. Earth Sci.* 3, 13–29. doi:10.15580/GJGES.2015.2.111915161

El-Taher, A. M., Aboul-Ella, H. A., Sayed, M. A., and Gaafar, A. A. (2004). Management of penile fracture. *J. Trauma Acute Care Surg.* 56, 1138–1140. doi:10.1097/01.ta.0000033140.73750.14

Firdaus, M. L., Minami, T., Norisuye, K., and Sohrin, Y. (2011). Strong elemental fractionation of Zr–Hf and Nb–Ta across the pacific ocean. *Nat. Geosci.* 4, 227–230. doi:10.1038/ngeo1114

Gaafar, I. M. (2005). Applications of geological and geophysical survey for defining the uranium potentiality of some younger granites in the Eastern Desert of Egypt. *J. Afr. Earth Sci* 2, 937–950.

Hassan, S. E. D., Fouda, A., Radwan, A. A., Salem, S. S., Barghoth, M. G., Awad, M. A., et al. (2019). Endophytic actinomycetes Streptomyces spp mediated biosynthesis of copper oxide nanoparticles as a promising tool for biotechnological applications. *JBIC J. Biol. Inorg. Chem.* 24, 377–393. doi:10.1007/s00775-019-01654-5

Hecht, L., Spiegel, W., and Morteani, G. (1994). Geochemistry and petrography of unaltered granites and their host rocks: fichtelgebirge granites. *Granites, Metallog.* 12, 143–177.

Howie, R. A., Zussman, J., and Deer, W. (1992). *An introduction to the rock-forming minerals*. London, UK: Longman.

Humphris, S. E. (1984). "The mobility of the rare earth elements in the crust," in *Developments in geochemistry* (Elsevier), 317–342.

Irber, W. (1999). The lanthanide tetrad effect and its correlation with K/Rb, Eu/Eu*, Sr/Eu, Y/Ho, and Zr/Hf of evolving peraluminous granite suites. *Geochim. Cosmochim. Acta* 63, 489–508. doi:10.1016/s0016-7037(99)00027-7

Jahn, B., Wu, F., Capdevila, R., Martineau, F., Zhao, Z., and Wang, Y. (2001). Highly evolved juvenile granites with tetrad REE patterns: the woduhe and baerzhe granites from the great xing'an mountains in NE China. *Lithos* 59, 171–198. doi:10.1016/s0024-4937(01)00066-4

Khamis, H. A., Ebyan, O. A., and Abed, N. S. (2020). Mineralogy and geochemistry of a new uranium occurrence at the decant of Wadi El reddah, northeastern desert, Egypt. *Nucl. Sci. Sci. J.* 9, 55–78. doi:10.21608/nssj.2020.265500

Krivovichev, S. V., Plášil, J., Burns, P. C., and Sigmon, G. E. (2013). Mineralogy and crystallography of uranium. *Uranium Cradle Grave. Mineral. Assoc. Can. Short Courses* 43, 15–119. doi:10.3749/9780921294689.ch03

López-Moro, F. J., Romer, R. L., Rhede, D., Fernández, A., Timón-Sánchez, S. M., and Moro, M. C. (2019). Early uranium mobilization in late Variscan strike-slip shear zones affecting leucogranites of central western Spain. *J. Iber. Geol.* 45, 223–243. doi:10.1007/s41513-018-0091-1

Lumpkin, G. R. (1998). Rare-element mineralogy and internal evolution of the Rutherford# 2 Pegmatite, Amelia County, Virginia; a classic locality revisited. *Can. Mineral.* 36, 339–353.

Mahdy, A. I., and El-Kammar, A. M. (2003). "Geochemical partitioning of isovalent and tetrad effect of REE associating episynitization of Kab Amiri granites, central Eastern Desert of Egypt," in *Proceedings of the 5th conference of geology of Middle East* (Cairo, Egypt: Spinger), 5–11.

Mason, B. (1952). *Principles of geochemistry*. LWW.

Mason, B., and Moore, C. B. (1991). *Principles of Geochemistry*. 4th Edn. New York, NY: Wiley Eastern Limited, 350.

Moghazy, N. M., El-Tohamy, A. M., Fawzy, M. M., Awad, H. A., Zakaly, H. M. H., Issa, S. A. M., et al. (2021). Natural radioactivity, radiological hazard and petrographical studies on aswan granites used as building materials in Egypt. *Appl. Sci.* 11, 6471. doi:10.3390/app11146471

Monecke, T., Kempe, U., Monecke, J., Sala, M., and Wolf, D. (2002). Tetrad effect in rare earth element distribution patterns: A method of quantification with application to rock and mineral samples from granite-related rare metal deposits. *Geochim. Cosmochim. Acta* 66, 1185–1196. doi:10.1016/s0016-7037(01)00849-3

Perişanoğlu, U., El-Agawany, F. I., Tekin, H. O., Kavaz, E., Zakaly, H. M. H., Issa, S. A. M., et al. (2021). Multiple characterization of some glassy-alloys as photon and neutron shields: in-silico Monte Carlo investigation. *Mater. Res. Express* 8, 35202. doi:10.1088/2053-1591/abeb4e

Peyronel, G. (1956). The crystal structure of Baveno bazzite. *Acta Crystallogr.* 9, 181–186. doi:10.1107/s0365110x56000401

Plasil, J. (2014). Oxidation-hydration weathering of uraninite: the current state-of-knowledge. *J. Geosci.* 59, 99–114. doi:10.3190/jgeosci.163

Recio, C., Fallick, A. E., Ugidos, J. M., and Stephens, W. E. (1997). Characterization of multiple fluid-granite interaction processes in the episyenites of Avila-Béjar, Central Iberian Massif, Spain. *Chem. Geol.* 143, 127–144. doi:10.1016/s0009-2541(97)00106-x

Rezaei Azizi, M., Abedini, A., Alipour, S., Niroomand, S., Sasmaz, A., and Talaei, B. (2017). Rare earth element geochemistry and tetrad effects in fluorites: A case study from the Qahr-Abad deposit, Iran. *Neues Jahrbuch für Geologie und Paläontologie–Abhandlungen*. 383, 255–273. doi:10.1127/njgpa/2017/0639

Rudnick, R. L., Gao, S., Holland, H. D., and Turekian, K. K. (2003). Composition of the continental crust. *crust* 3, 1–64.

Saudi, H. A., Tekin, H. O., Zakaly, H. M. H., Issa, S. A. M., Susoy, G., and Zhukovsky, M. (2021). The impact of samarium (III) oxide on structural, optical and radiation shielding properties of thallium-borate glasses: experimental and numerical investigation. *Opt. Mater. (Amst).* 114, 110948. doi:10.1016/j.optmat.2021.110948

Schoep, A. (1921). La curite, nouveau minéral radioactif. *Compt. Rend. Hebd. Séan. Acad. Sci. Paris* 173, 1186–1187.

Stemprok, M. (1979). Mineralized granites and their origin. *Episodes J. Int. Geosci.* 2, 20–24. doi:10.18814/epiiugs/1979/v2i3/005

Taalab, S. A., Abdel-Rahman, A. M., El-Awny, H., Awad, H. A., Zakaly, H. M. H., Fahmy, W., et al. (2023b). Petrogenesis and tectonic evolution of Kab Amiri ophiolites and island-arc assemblages, central Eastern Desert, Egypt: petrological and geochemical constraints. *Minerals* 13, 528. doi:10.3390/min13040528

Taalab, S. A., Mohamed, W. H., Shetaia, S. A., Al Meshari, M., Alzamil, Y., Abanomy, A., et al. (2023a). Radiological and environmental hazards of granitic rocks in Wadi faliq El sahl and El waar area, north Eastern Desert, Egypt. *J. Environ. Sci. Health Part A* 58, 326–341. doi:10.1080/10934529.2023.2186650

Taran, M. N., Dyar, M. D., Khomenko, V. M., and Boesenberg, J. S. (2017). Optical absorption, Mössbauer, and FTIR spectroscopic studies of two blue bazzites. *Phys. Chem. Min.* 44, 497–507. doi:10.1007/s00269-017-0877-2

Tarrah, J. (2016). Normative calculation of mineral composition in Cr ores of the ophiolite complexes from SE Iran. *J. Earth Sci.* 8, 36–44.

Tartèse, R., Boulvais, P., Poujol, M., Gloaguen, E., and Cuney, M. (2013). Uranium mobilization from the Variscan Questembert syntectonic granite during fluid-rock interaction at depth. *Econ. Geol.* 108, 379–386. doi:10.2113/econgeo.108.2.379

Tekin, H. O., Ali, F. T., Almisned, G., Susoy, G., Issa, S. A. M., Ene, A., et al. (2022). Multiple assessments on the gamma-ray protection properties of niobium-doped borotellurite glasses: A wide range investigation using Monte Carlo simulations. *Sci. Technol. Nucl. Install.* 2022, 1–17. doi:10.1155/2022/5890896

Tekin, H. O., Erguzel, T. T., Sayyed, M. I., Singh, V. P., Manici, T., Altunsoy, E. E., et al. (2018). An investigation on shielding properties of different granite samples using MCNPX code. *Dig. J. Nanomater. Biostructures* 13 (2), 381–389.

Van Schmus, W. R. (2013). "Natural radioactivity of the crust and mantle," in *Global earth physics: A handbook of physical constants* (Wiley Online Library), 283–291. doi:10.1029/rf001p0283

Tischendorf, G. (1977). Geochemical and petrographic characteristics of silicic magmatic rocks associated with rare-metal mineralization. Metallization Associated with Acid Magmatism. *Sci. Res.* 2, 41–98.

Watanabe, Y., Sato, R., and Sulaksono, A. (2018). Role of potassic alteration for porphyry Cu mineralization: implication for the absence of porphyry Cu deposits in Japan. *Resour. Geol.* 68, 195–207. doi:10.1111/rge.12165

Zakaly, H. M. H., Alsaif, N. A. M., Shams, · M. S., El-Refaey, A. M., Elsad, · R. A., Sadeq, · M. S., et al. (2023). Synthesis, physical, optical characteristics, neutron/γ-rays shielding capacity of newly arsenic glasses: experimental, theoretical, and simulation investigations. *Opt. Quantum Electron.* 554 (55), 365–425. doi:10.1007/S11082-023-04610-5

Zakaly, H. M. H., Saudi, H. A., Tekin, H. O., Rashad, M., Issa, S. A. M., Rammah, Y. S., et al. (2021). Glass fabrication using ceramic and porcelain recycled waste and lithium niobate: physical, structural, optical and nuclear radiation attenuation properties. *J. Mater. Res. Technol.* 15, 4074–4085. doi:10.1016/J.JMRT.2021.09.138

Zakaly, H. M. H., Tekin, H. O., Issa, S. A. M., Henaish, A. M. A., Ahmed, E. M., and Rammah, Y. S. (2022). Fabrication, physical, structure characteristics, neutron and radiation shielding capacity of high-density neodymio-cadmium lead-borate glasses: nd2O3/CdO/PbO/B2O3/Na2O. *Appl. Phys. A Mater. Sci. Process.* 128, 551–617. doi:10.1007/s00339-022-05689-5

Zhang, J., Amakawa, H., and Nozaki, Y. (1994). The comparative behaviors of yttrium and lanthanides in the seawater of the North Pacific. *Geophys. Res. Lett.* 21, 2677–2680. doi:10.1029/94gl02404